Chemical Engineering Journal 430 (2022) 131000

Contents lists available at ScienceDirect

Chemical Engineering Journal

journal homepage: www.elsevier.com/locate/cej

Heat transfer intensification with packed open-cell foams in TSA processes for CO_2 capture

Stefano E. Zanco [a], Matteo Ambrosetti [b], Gianpiero Groppi [b], Enrico Tronconi [b], Marco Mazzotti [a,*]

[a] Institute of Energy and Process Engineering, ETH Zurich, 8092 Zurich, Switzerland
[b] Department of Energy, Politecnico di Milano, Milano, Italy

ARTICLE INFO

Keywords:
TSA
Packed foam
Open-cell foam
CO_2 capture

ABSTRACT

Packed open-cell foams are proposed as an alternative to standard packed bed configuration commonly adopted for the adsorption columns of a temperature swing adsorption process. In this contribution, heat transfer in an adsorption column with a packed foam configuration is investigated by experimental and modeling analysis, in comparison to a standard packed bed. The introduction of the packed foam allows for more rapid temperature transitions and substantial reduction of temperature gradients within the adsorption bed. The impact of this heat transfer enhancement on the separation performance of a temperature swing adsorption process is evaluated by modeling an example post-combustion CO_2 capture application. Although the presence of the foam implies a loss of sorbent inventory (-26.5%), higher process productivity (+80%) is achieved thanks to faster temperature swings and more homogeneous temperature distribution within the adsorption columns.

1. Introduction

Among adsorption based separations, Temperature Swing Adsorption (TSA) processes include all those processes, commonly performed in fixed bed gas-solid contactors, where the regeneration of the solid sorbent is enabled by an increase in temperature of the system. The interest in this type of processes has noticeably risen over the last decades in parallel with the research on the reduction of greenhouse gas emissions, a purpose for which they have been identified as an interesting alternative to widely studied scrubbing processes using aqueous amine solutions as solvent [1,2].

The application of TSA processes to the treatment of large gas flow rates, like the ones usually involved in post-combustion CO_2 capture from flue gas, has highlighted how this type of processes suffer from low productivity, defined as the capacity of separation of the desired product per unit plant footprint and unit operation time. The reason of this limitation has been identified with slow heat transfer kinetics, an intrinsic feature of the fixed bed contactors operated with the aim of gas separation, which play a rate-limiting role in the heating and cooling phases of a cyclic TSA operation [3].

Several solutions have been proposed to overcome this limitation: bed configurations alternative to the fixed bed (rotary beds [4], fluidized beds [5,6]), alternative heating approaches (electrical heating [7], direct heating [8], microwave heating [9]); structured sorbent with a shape different than the pellets adsorption column are commonly packed with (both supported or self-supported [10–13]). Among structured sorbents and in the context of CO_2 capture, particularly interesting are the so-called Rapid TSA systems where the sorbent is either embedded in a polymeric hollow fiber support [3] or formed into self-supported monoliths [14,15]. On the one hand, these systems have demonstrated to partially overcome heat transfer limits, thus enabling for extremely fast cycling; on the other hand, the production of these structures is not always economical, and the sorbent inventory they can attain is often smaller than that of columns filled with pellets.

The topic of heat transfer limitations is of great relevance in catalytic applications as well. Multitubular reactors with diameters in the range 2–15 cm packed with pellets and indirectly heated or cooled are widely employed in catalytic processes. These systems are typically operated at high flow velocities for the combined needs of productivity, adequate contact time to reach target conversions, and efficient heat transfer to enable effective process temperature control [16]. A related issue is that these solutions are not viable for a scale down of the process: When reducing the tube length, the flow velocity scales down and the heat transfer performance worsens, because the convective mechanism that governs heat transfer is suppressed [17].

Several kinds of washcoated structured catalysts [18] (conductive honeycombs [19], wire meshes [20], foams [21,22]) or packed systems (packed monoliths [23], packed foams [24,25]) have been proven effective to overcome heat transfer limitations. In particular, the use of packed foams and of packed periodic ordered geometries has been

* Corresponding author.
E-mail address: marco.mazzotti@ipe.mavt.ethz.ch (M. Mazzotti).

https://doi.org/10.1016/j.cej.2021.131000
Received 10 May 2021; Received in revised form 18 June 2021; Accepted 19 June 2021
Available online 25 June 2021

demonstrated as a suitable solution for the intensification of energy-intensive processes like methane steam reforming [21,25] and Fischer–Tropsch synthesis [24].

Thanks to the adoption of highly conductive materials, these packed structures outperform standard packed bed configurations in terms of heat transfer kinetics in tubular reactors, especially at low flow rate conditions, while they can house comparable catalyst inventories. The non-ordered version of these packed structures, the open-cell foams, features a combination of bulk materials with high thermal conductivity and interconnected frames throughout the reactor volume [26], thus providing an effective thermal conductivity in the radial as well as in the axial direction. The heat transfer mechanism of the packed open-cell foams has been investigated in recent studies, where an electrically equivalent network of heat transfer resistances has been developed to derive an overall heat transfer coefficient as a function of the packing geometry and of the operating conditions [25].

Given the strong analogies between catalytic and adsorption processes, there is a potential for these concepts to be successfully employed also in adsorption processes [27]. In this work, we report the – to the best of our knowledge – first experimental analysis of the application of packed open-cell foams to TSA processes, applied to a post-combustion carbon capture process using Zeolite 13X as sorbent. The performance of the packed foam (PF) is assessed through the comparison with a standard packed bed (PB) configuration. First, heat transfer performances have been tested. Thereafter, the experimental rig has been operated for the main step of a TSA cycle, to estimate the benefits in terms of separation performance. Finally, a one-dimensional model is used to investigate the overall efficiency of an optimized CO_2 capture process with the packed foam. Our results show that, consistently with the expectations, the heat transfer properties of open-cell foams help in achieving a more homogeneous temperature distribution and faster column dynamics during operation, hence allowing for faster cycling of a TSA process. This benefit overcompensates a partial loss of adsorption capacity, eventually resulting in a substantial increase of process productivity, at the inevitable cost of a slightly higher energy consumption.

2. Experimental setup

2.1. Adsorption column

In order to observe neatly distributed radial temperature profiles developed both at steady state and under transient conditions, a cylindrical adsorption column with a large diameter of 80.2 mm has been built in house.

The column, 800 mm long (length-to-diameter ratio of 10, to allow for full development of a plug flow velocity profile), is divided into two sections (600 mm and 200 mm, respectively; Fig. 1a), the top one hosting the adsorbent bed of Zeolite 13X (ZeoChem, Switzerland), the bottom part housing an inert packing of glass beads of the same size and shape of the adsorbent (2.00 mm, spherical). With this configuration, a limited amount of sorbent is used (approximately 1 l) in order to reduce the duration of the breakthrough experiments.

The adsorber section of the column is jacketed. In the jacket, a continuous flow of silicon oil works as indirect heat source or heat sink. Two different oil streams may circulate in the external jacket, each of them being temperature-controlled by a dedicated thermostat (Huber AG, Switzerland), one set on a low temperature (i.e. 25 °C) and one at a suitable temperature to perform heating experiments or bed regeneration. While one stream is conveyed through the column jacket, the other flows through a bypass, and the two can be switched by means of automated valves to quickly adjust the temperature in the adsorber, from heating to cooling and vice versa.

K-type thermocouples (Moser TMT AG, Switzerland) are installed longitudinally at three different positions along the radial direction, namely at the center, close to half-radius length, and close to the vessel wall (Fig. 1b). These three can slide along the axial direction for most of the bed length to obtain a 2D temperature map during steady-state heat transfer experiments, whilst they are kept at a fixed position (60% of the bed length, 120 mm from adsorption bed inlet) during transient experiments. An additional thermocouple is installed transversely 32.0 mm below the interface between the two sections, to measure the temperature of the gas entering the adsorbent bed.

The gas mixtures (Pangas AG, Switzerland) are fed to the column while controlling the inlet flow rate with a mass flow controller (Bronkhorst, Netherlands), whereas at the column outlet a mass flow meter (Bronkhorst, Netherlands) and a mass spectrometer (Pfeiffer, Germany) measure flow rate and gas composition, respectively. Temperature and pressure are measured upstream and downstream of the column with additional K-type thermocouples and pressure transducers (Keller, Germany).

2.2. Column packing

The same column has been used to perform all the experiments, with and without metal foams.

The used adsorbent particles all belonged to the same production batch of those characterized by Hefti et al. [28] and Marx et al. [29] through equilibrium and kinetic experiments. The beads (nominal average size: 2.0 mm) have been sieved to separate the particles with diameter smaller than 2.00 mm. During the packing operations, the particles have been exposed to air (at approximately 23 °C, 25% RH). After the packing and prior to the experiments, the bed has been regenerated by heating and under vacuum (150 °C, 0.005 bar) for 12 h.

For the packed bed (PB) experiments, larger particles (average diameter: 2.00 mm) have been packed within the column by simply pouring them and packing them tightly with the aid of a vibrating support. A final void fraction of 0.388 has been determined from the amount of sorbent loaded in the column (as expected for this specific tube to particle diameter ratio), corresponding to a zeolite inventory of 664 kg/m^3 (measured after exposure to air).

The foam has been characterized with optical microscopy to determine the cell size, whereas its porosity has been determined by gravimetric measurements coupled with ethanol picnometry, determining a void fraction of 0.95 and an average cell size equal to 5.0 mm. For the packed foam (PF) experiments, a series of disks (40.0 mm high, 80.1 mm in diameter) have been shaped out of a pure-aluminum foam sheet by high-precision cutting (Electro Discharge Machining — EDM), and bored with holes to house the thermocouples in the positions described before. The disks have been first placed within the vessel and filled with slightly smaller particles (average diameter: 1.78 mm) layer by layer with the aid of a vibrating support (Figs. 2a and 2b). The final packing has resulted into a void fraction of 0.485 (defined on the residual void space in the column after placing the foam), also confirmed by preliminary measurements performed outside of the column and consistent with previous works performed at Politecnico di Milano [30], corresponding to an inventory of zeolite of 531 kg/m^3 (measured after exposure to air).

Considering that the particles have been exposed to moist air, the mass measured during the packing likely includes a certain amount of adsorbed water. Since its presence is highly detrimental for the adsorption capacity of other species, as shown by Hefti and Mazzotti [31], it is important to determine the amount of adsorbed water loaded on the sorbent in order to forecast the right adsorption capacity for CO_2.

According to the water isotherms measured by Hefti and Mazzotti on the very same adsorbent, at equilibrium conditions at 25% relative humidity Zeolite 13X can adsorb approximately 15.4 mol of water per kg of particles, which corresponds to an apparent mass increase of the solid inventory of 27.9%. However, due to the slow kinetics of water adsorption on zeolites, it is unsure that equilibrium conditions have been reached during the exposure time. Moreover, it cannot be excluded that, even after a long regeneration time, at 150 °C all the

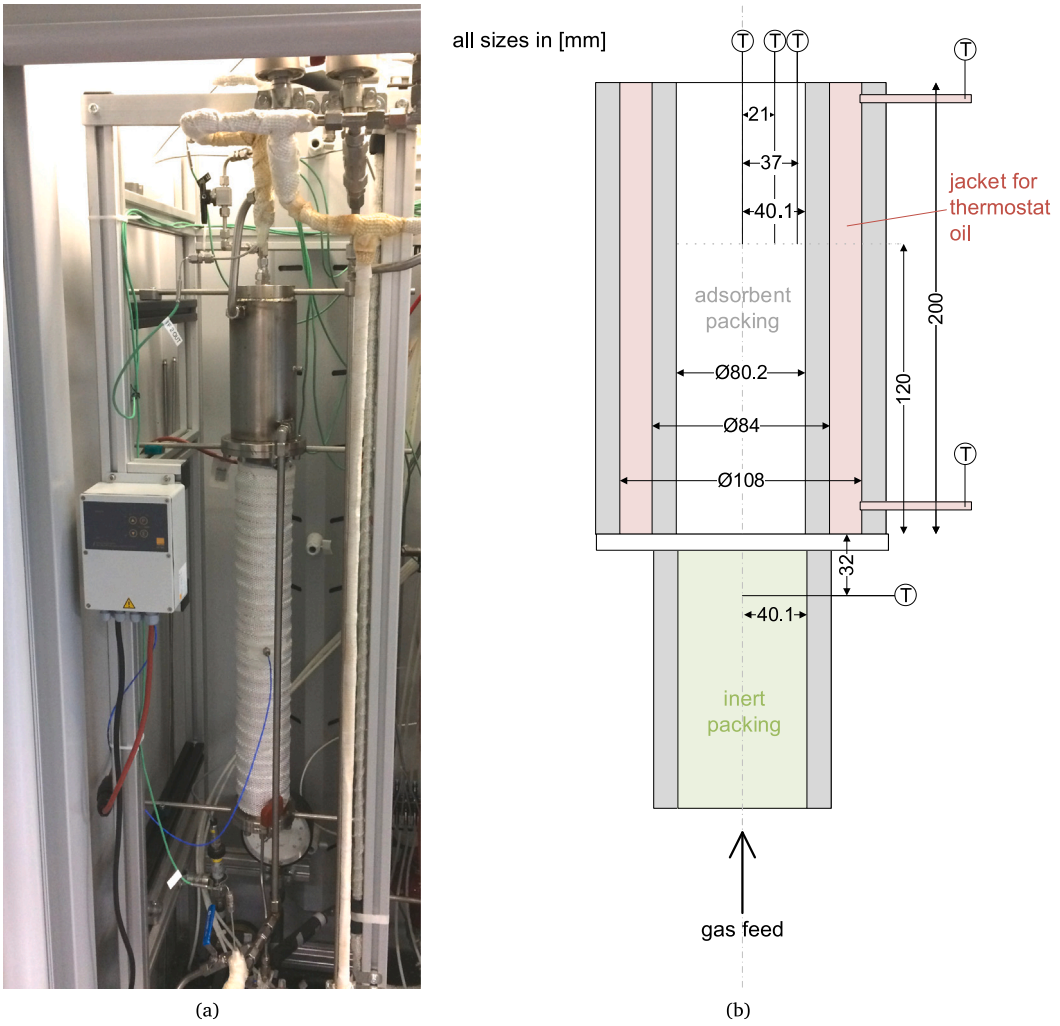

(a) (b)

Fig. 1. Experimental setup with large cross-section adsorption column. (a) Adsorption column installed within the rig and connected to the heating/cooling system and the gas feeding system. The top part with the steel jacket is packed with the adsorbent beads, while the lower part (covered by a thermo-insulating tape) is packed with inert glass beads. (b) Scheme of the adsorber section of the column.

moisture adsorbed is released, thus recovering full capacity for the adsorption of CO_2.

In order to determine the real mass of zeolite packed for the two configurations, after the experiments the solid inventories have been unpacked from the column, weighed again (686 and 534 kg/m^3 of pellets, for PB and PF respectively), and finally sampled by means of thermogravimentric analysis (TGA). During the TGA measurement, the two samples (one from the PB packing, one from the PF one) have been exposed to an atmosphere of pure N_2, whose adsorption capacity on Zeolite 13X can be considered negligible at high temperatures, heated up progressively to 600 °C (at a heating rate of 10 °C/min) and then left at this temperature for additional 20 min. The mass decrease of the samples as a function of temperature, as measured during the TGA, is shown in Fig. 3. From this measurement, the net total zeolite inventory has been estimated to be 562 and 413 kg/m^3, for PB and PF, respectively. The difference in the mass variation observed during the two TGA measurements is justified by the fact that the two inventories have been unpacked in different moments, after being exposed first to different experimental conditions and later to ambient air for different periods of time.

In total, the introduction of the metal foam causes a loss of sorbent inventory of 26.5%, thus implying a corresponding reduction of the capacity for adsorption per unit column volume.

It is also worth noting that the total heat capacity is virtually the same for the two configurations: In the PF case, the lower sorbent inventory is compensated by an almost equal mass of aluminum (135 kg/m^3), which has a very similar specific heat capacity as that of the zeolite, as reported in Table 1. Therefore the absolute thermal capacity of the two systems is comparable.

3. Heat transfer measurements

In a standard PB configuration, heat transfer relies mainly on two mechanisms, namely the conduction through the gas and solid phase, and the convection due to the fluid flow. Due to the relatively low temperatures reached in the application that is object of this study, radiation can be neglected. Under flow conditions typical of packed bed reactors (Reynolds number large than 50), the convective contribution neatly predominates due to the poor thermal conductivity of the pellets and the absence of radial and axial continuity of the solid material. As a consequence, the effectiveness of the temperature control in the system, as applied from an indirect heat source or sink, strongly depends on the fluid dynamics of the gas, and is particularly hindered in absence of flow, e.g. during the heating and cooling transitions, that end up in representing the bottleneck steps in cyclic processes.

It has been demonstrated, instead, that in a packed foam configuration the heat transfer mechanisms of a standard packed bed are

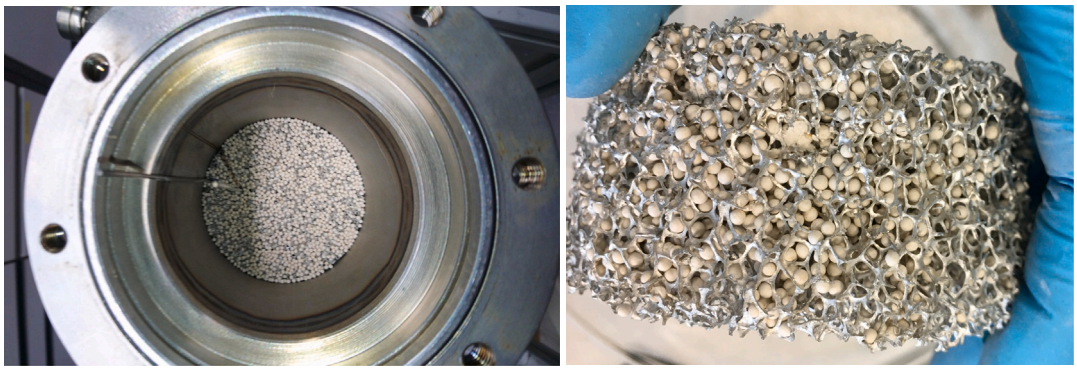

(a) (b)

Fig. 2. Pictures of the metal foam packing with zeolite beads. (a) Adsorption column with the first disks of foam inserted and packed with zeolite beads, before the experiments. (b) Detail of a foam disk packed with zeolite beads. Picture taken while dismantling the column packing, after the experiments.

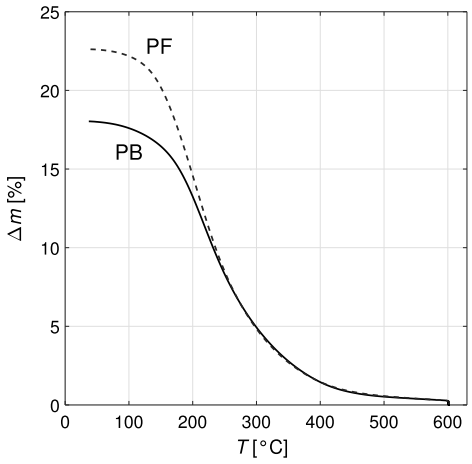

Fig. 3. Relative mass difference (to the final measured mass) as a function of the temperature to which the samples are exposed during the TGA measurement.

assisted by those of the open-cell foam metal frame [25,32], which shows high effective thermal conductivity thanks to both the solid continuity [26] and a material conductivity four orders of magnitude higher than that of the sorbent beads (see Table 1). As a consequence, the insertion of the foam within the column allows not only to reduce the overall thermal resistance within the adsorption column, but also to switch from a mainly convective to a mainly conductive heat transfer mechanism. Since conduction through the solid phase is not affected by the gas flow, higher thermal conductivities entail advantages especially at low-velocity operating conditions.

The expected benefits are twofold: On the one hand, thermal transitions are supposed to occur faster; on the other hand, the reduced thermal resistance should flatten out both the axial and the radial temperature gradients, enabling a more precise control of the temperature across the adsorbent bed, thus with a potential increase in the adsorption capacity.

To evaluate the thermal response of the adsorption column in the two different configurations, measurements have been performed under inert conditions. Argon (99.995% vol. purity) has been chosen as inert gas, given its similarities to CO_2 in terms of molar mass, heat capacity and thermal conductivity. Heat transfer in the column has been assessed by means of two types of experimental observations:

1. Analyzing the temperature profiles, both in the axial and in the radial direction within the column once the system has reached steady state and the column is continuously heated from the jacket and fed with cold inert gas at different flow rates by moving the thermocouples inside the bed.

Table 1
Experimental setup and materials.

Adsorption column vessel	
Material	Stainless steel, type 1.4404
Wall thickness	1.9 mm
Inner diameter, D_{in}	80.2 mm
Inert bed length	600.0 mm
Adsorbent bed length	200.0 mm
Thermocouple radial positions:	
Central	0.0 mm
Half-radius length	21.0 mm
Close to wall	37.4 mm
Material density	10 000 kg/m^3
Heat capacity	400 J/kg/K
Thermal conductivity	60 W/m/K
Adsorbent	
Material	Zeolite 13X
Pellet shape	Spherical beads
Pellet size D_{50} PB, d_p	2.00 mm
Pellet size D_{50} PF, d_p	1.78 mm
Material density	2359 kg/m^3
Particle density, ρ_p	1085 kg/m^3
Bed inventory PB (after exposure to air)	664 kg/m^3
Bed inventory PB (regenerated), ρ_{PB}	562 kg/m^3
Bed inventory PF (after exposure to air)	531 kg/m^3
Bed inventory PF (regenerated), ρ_{PF}	413 kg/m^3
Heat capacity	920 J/kg/K
Thermal conductivity, k_p	0.17 W/m/K
Metal foam	
Material	Aluminum
Void fraction, ε_F	0.95
Average cell diameter, D_{cell}	5.0 mm
Aluminum inventory	135 kg/m^3
Material density	2710 kg/m^3
Heat capacity	900 J/kg/K
Thermal conductivity, k_F	200 W/m/K

2. Analyzing the dynamic evolution of the temperature within the column, when it undergoes a step change of temperature of the indirect heating and cooling system by keeping thermocouples in a fixed bed position. These experiments have been performed both at zero flow conditions at different pressures, and under flow conditions, feeding cold inert gas at different flow rates.

3.1. Steady state temperature profiles

The first set of measurements was aimed at the observation of the temperature gradients within the column at steady state. To perform these experiments, cold Ar has been fed at flow rates between 12.5 and 81 nL/min (normal liter per minute, referred to $T = 0$ °C, $P = 1.01325$ bar).

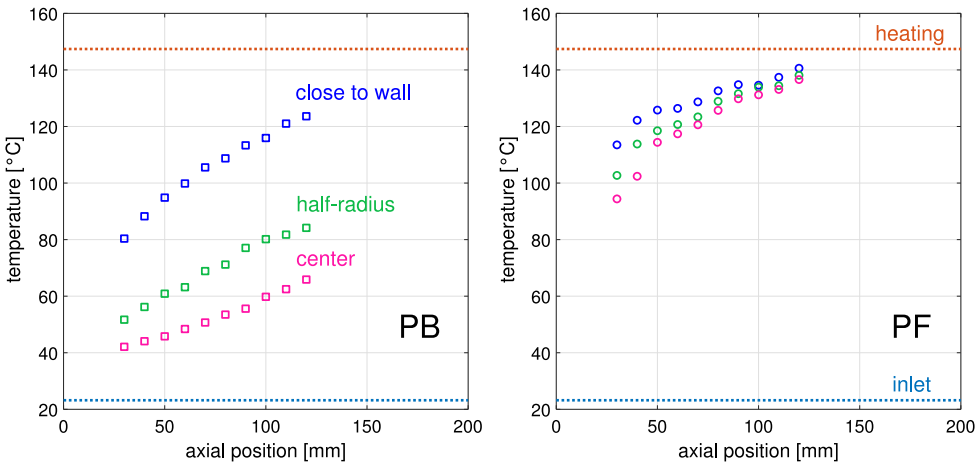

(a) Packed bed (b) Packed foam

Fig. 4. Axial temperature profiles at steady state during heating at 150 °C while feeding Ar at 25 °C at 25 nL/min. The colors indicate the position of the thermocouples: central (magenta, $r = 0$ mm), half-radius (green, $r = 21$ mm) and close to wall (blue, $r = 37.1$ mm). The dotted lines indicate the temperature of the oil flowing in the heating jacket (red) and the gas inlet temperature (blue).

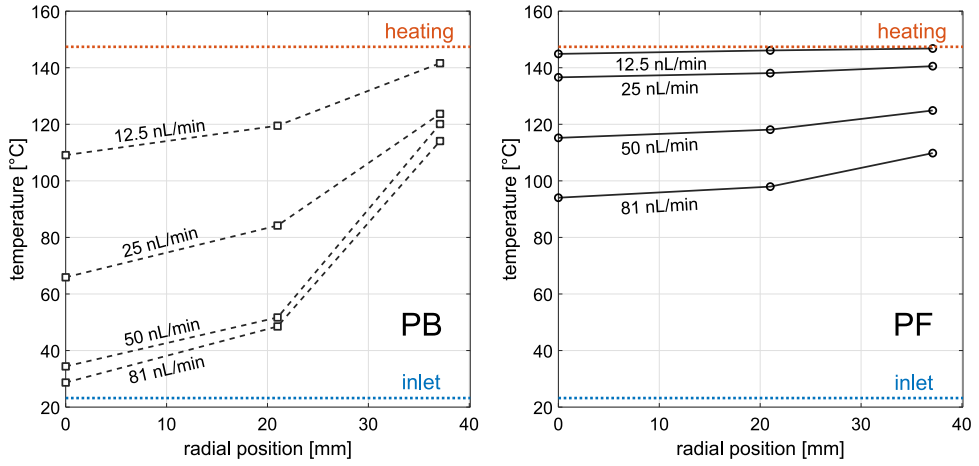

(a) Packed bed (b) Packed foam

Fig. 5. Radial temperature profiles at steady state during heating at 150 °C while feeding Ar at 25 °C at different flow rates. The three thermocouples are placed at 120 mm from the inlet of the adsorbent bed, at different radial positions corresponding to the positions indicated in Fig. 4: central ($r = 0$ mm), half-radius ($r = 21$ mm), and close to wall ($r = 37.1$ mm). The dotted lines indicate the temperature of the oil flowing in the heating jacket (red) and the gas inlet temperature (blue).

Under flow conditions, the observed temperature profiles are characterized by temperature gradients both in the axial direction and in the radial direction. The heat is provided transversely to the flow direction from the column wall, and transferred toward the center of the column by a mixed conductive–convective heat transfer mechanism, while being transported along the column by advection. This prevents the adsorbent bed from reaching the wall temperature, and causes the development of axial temperature gradients due to the progressive heating of the gas stream. After waiting for the thermal steady-state, the measurements were performed.

In Fig. 4 the temperatures measured at the three radial positions and at different axial positions (from 30 mm to 120 mm from the column inlet) are shown. In order to perform this measurement, the inert gas has been fed constantly at 25 °C while applying a heating step (from 25 to 150 °C) to the column. Once at steady state, the thermocouples have been shifted along the axial direction, so as to measure the temperatures at different axial positions. As expected, the temperature always increases from the center of the column toward the wall, where the heat is provided to the bed. In the PB case, the three temperature profiles are neatly separated, while in the PF case they are closer to each other and to the temperature of the external heating fluid, as a consequence of the reduced thermal resistance of the system.

The observation of the profiles suggests that the radial gradients reach a maximum extent at a certain axial position, while they are flat at the inlet (where the gas is fed at uniform temperature) and tend to flatten out toward the outlet. The position of the maximum gradient mainly depends on the ratio between the amount of heat conveyed by advection by the gas flow and the amount of heat exchanged radially through the bed. Since the gas flow rate is the same in the two measurements (and thus the heat advection terms), the fact that this maximum gradient is reached for this specific flow conditions at around 9 cm from the inlet for the PB and 4 cm for the PF further proves that heat transfer in the radial direction is significantly enhanced in the PF configuration for low Re and large column diameters.

The temperature gradients in the radial direction at 120 mm from the column inlet are displayed in Fig. 5 for four different gas flow rates, in order to show the influence of the gas velocity on the temperature distribution within the column.

The advective term of heat transfer becomes larger with increasing velocity, implying that with a cold feed the larger the flow rate, the lower the average temperature in the bed, provided that heat convection increases less than proportionally with the velocity. The comparison between the measurements highlights though a neat difference in the impact of the velocity on the radial temperature gradients,

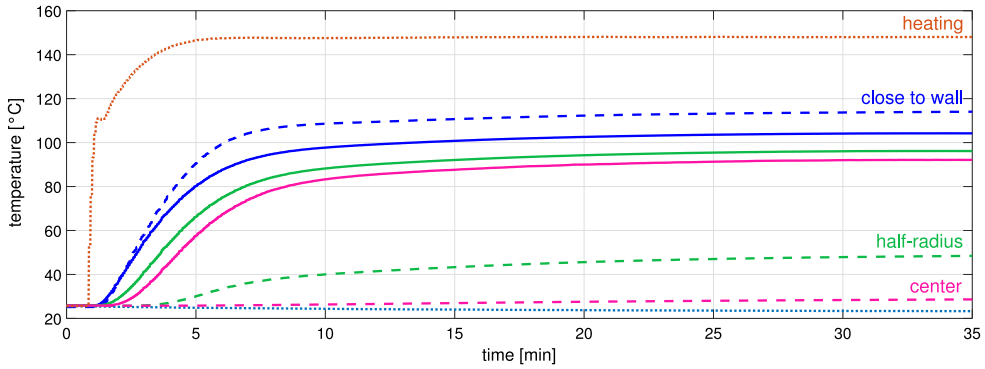

Fig. 6. Dynamic evolution of the temperature within the column as measured by the three thermocouples placed at 120 mm from the inlet of the adsorbent bed, during a temperature change from 25 °C to 150 °C with a flow rate of 81 nL/min of Ar at 25 °C. The dashed lines indicate the measurements in the packed bed. The solid lines indicate the measurements in the packed foam. The colors indicate the position of the thermocouples: central (magenta), half-radius (green) and close to wall (blue). The dotted lines indicate the temperature of the oil flowing in the heating jacket (red) and the gas inlet temperature (blue).

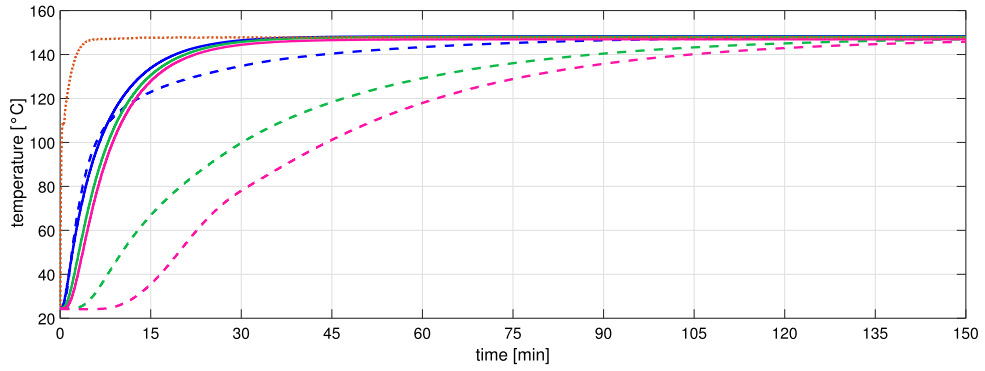

Fig. 7. Dynamic evolution of the temperature within the column as measured by the three thermocouples placed at 120 mm from the inlet of the adsorbent bed, during a heating transition from 25 °C to 150 °C under continuously drawn vacuum from the column (at 5 mbar). The dashed lines indicate the measurements in the packed bed. The full lines indicate the measurements in the packed foam. The colors indicate the position of the thermocouples: central (magenta), half-radius (green) and close to wall (blue). The dotted red line indicates the temperature of the oil flowing in the jacket.

in the range of tested flow rates. For the PF case, the temperature difference measured between the central thermocouple and the one close to the wall is always significantly smaller (in general, less than 20% compared to the PB case), the profiles are flatter, and the average temperature decreases progressively with the velocity. In the PB case, the parabolic shape of the temperature profiles is more pronounced, and already at 50 nL/min the heat transfer limitations lead almost to a negligible temperature increase on the internal temperature measurements.

In general, the average temperature of the bed is considerably higher with the foam at any flow rate, and a more homogeneous distribution of the heat across the cross section is achieved.

3.2. Dynamic temperature profiles

Being the two systems characterized by comparable thermal capacities, a faster transition to the steady state is expected for the system exhibiting higher heat transfer rates.

Fig. 6 shows the dynamic evolution of the three temperatures measured by the thermocouples during a step change of temperature of the heating system. To reproduce operations in a temperature swing, cold oil (25 °C) flow has been initially conveyed through the column jacket; then suddenly the cooling stream and the heating stream of oil have been switched. As it can be seen from the figure, the temperature of the external fluid changes quickly and stabilizes in approximately 5 min at its final setpoint (150 °C). For the whole duration of the measurement, a flow of cold Ar (81 nL/min, 25 °C) has been continuously fed to the column inlet.

The two systems display a steady state temperature distribution after approximately 12 and 9 min for the PB and PF, respectively. However, the temperatures keep rising further, most likely due to secondary phenomena associated with the slow heating of the surrounding metal parts of the setup, and the consequent further increase of the wall temperature close to the column inlet. After approximately 35 min, the ultimate steady state (as reported in Fig. 5) is reached.

The homogeneity of the temperature distribution across the radius is the most evident feature of the PF configuration. Once the steady state is reached, the difference between the temperature in the center of the column and that close to the wall is 85.4 °C and 12.1 °C for the PB and the PF, respectively. This highlights the predominant role played by the metal foam in transferring heat and thus limiting the internal temperature gradients.

The benefits deriving from an increased conduction through the bed are even more evident in absence of flow, as demonstrated by Ambrosetti et al. [33]. Temperature step experiments have been performed at zero gas velocity at close to ambient pressure (in Ar) and under vacuum, all yielding the same results. In Fig. 7 the dynamic evolution of the temperatures for the same heating step under vacuum is shown. Here, given the absence of flow, the whole column is brought to the same temperature at steady state, and radial gradients can be observed during the transient phase of the experiment.

The PB responds to the change of oil temperature with slow dynamics. The distance between the curves of the three thermocouples demonstrates how the conduction through the zeolite beads alone has difficulties in transferring heat to the center of the bed. In total, the system needs more than 150 min to reach the thermal steady state. The PF, instead, stabilizes at the highest temperature after only 48 min,

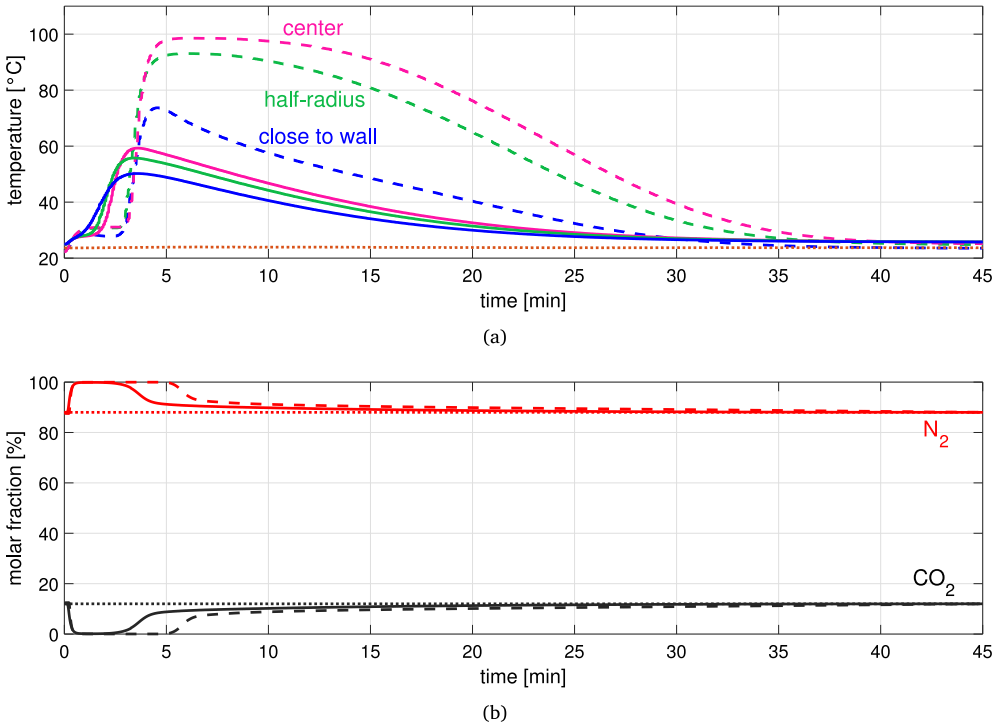

Fig. 8. Breakthrough experiment. A binary mixture of CO_2/N_2 (12/88% vol.) is fed at 35 nL/min and 25 °C. (a) Dynamic evolution of the temperature within the column as measured by the three thermocouples placed at 120 mm from the inlet of the adsorbent bed. The dashed lines indicate the measurements in the packed bed. The full lines indicate the measurements in the packed foam. The colors indicate the position of the thermocouples: central (magenta), half-radius (green) and close to wall (blue). The dotted red line indicates the temperatures of the oil flowing in the jacket. (b) Dynamic evolution of the gas composition at outlet, as measured by the mass spectrometer. The dashed lines indicate the measurement in the packed bed. The full lines indicate the measurement in the packed foam. The colors indicate the two species of the binary mixture, namely CO_2 (black) and N_2 (red). The dotted lines indicate the gas composition at inlet.

with a reduction of about 70% of the transition time, and restrains the formation of radial temperature gradients for the whole duration of the experiment.

4. Adsorption measurements

To assess the impact of the two different heat transfer regimes on the separation performance of the adsorption column, breakthrough experiments with a CO_2-N_2 mixture (12%–88% vol.) have been performed. The gas mixture has been fed until saturation of the bed and further (duration: 60 min), giving time to the system to re-stabilize at its initial temperature (25 °C). Two different flow rates have been tested, 35 and 70 nL/min. Thereafter, regeneration at high temperature (120 min) and a successive cooling (180 min) of the column have also been measured following a systematic procedure, to reproduce the most relevant steps of a TSA process. During regeneration and cooling, no gas has been fed to the column; during the former, the bottom end of the column has been left open to allow for gas evacuation, whereas during cooling both ends of the column have been kept close. Three different regeneration temperatures (120, 150, and 200 °C) have been tested. Between each series of experiments (adsorption, regeneration, cooling) the column has been regenerated by heating and drawing vacuum (150 °C, 0.005 bar) for 12 h.

4.1. Adsorption breakthrough

Fig. 8 shows the dynamic evolution of the simultaneous measurements of the three thermocouples (Fig. 8a) and of the mass spectrometer (Fig. 8b) during an adsorption breakthrough experiment performed with the smaller gas flow rate, 35 nL/min.

The different heights of the temperature fronts can be readily observed. The measurements of the three thermocouples always deviate by less than 15 °C with the PF, which become more than 40 °C in the PB case. This shows how the radial temperature distribution within the column is flattened out. Although not directly shown by these measurements, this is also true in the axial direction, as it can be inferred by the more pronounced spreading of the temperature waves in the PF, compared to the steeper fronts observed with the PB.

It can also be immediately observed how the CO_2 breaks through earlier in the PF case, as clearly demonstrated by both the concentration front at the column outlet and the temperature front within the column. This is expected, consistently with the loss of sorbent inventory mentioned in Section 2, which is intrinsic of the packed foam configuration. Moreover, the spreading of the temperature front coincides with a smoother concentration profile at the outlet, which is undesirable in adsorption processes. On the contrary, the shorter and shallower tail of the temperature wave enables a faster saturation of the sorbent capacity, and corresponds to a higher average loading in the column at breakthrough. This is confirmed by the elbow formed by the concentration front at breakthrough: The point where the profile bends and flattens toward the feed concentration occurs at a higher CO_2 concentration in the PF case, thus implying that the adsorption capacity has been exploited better up to that point. This is clearly consistent with the lower average temperature reached within the column.

Although the most obvious reason of the shorter breakthrough time lies in the lower sorbent inventory housed by the foam, the calculation of the total adsorbed amounts of CO_2 during the breakthrough experiments produces unexpected results. This calculation is done by integration of the inlet and outlet flow rates of the single species, i.e.

$$q_{\mathrm{tot,CO_2}} = \int_0^{t_{\mathrm{ads}}} \left(F_{\mathrm{in}}\, y_{\mathrm{in,CO_2}} - F_{\mathrm{out}}(t)\, y_{\mathrm{out,CO_2}}(t) \right) \mathrm{d}t \tag{1}$$

It returns values close to the prediction of the extended Sips isotherm for the PB case, whereas it shows a consistent reduction of the total adsorbed amount $q_{\mathrm{tot,CO_2}}$ of 40%–45% from the PB to the PF case throughout all breakthrough curves, which is significantly higher than

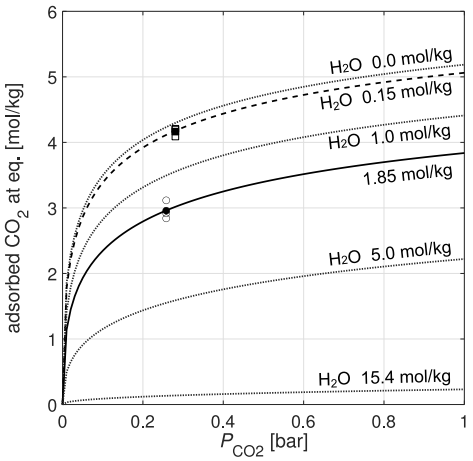

Fig. 9. Adsorption of CO_2 on Zeolite 13X pre-loaded with water at 25 °C [31]. The writings indicate the amount of pre-loaded water. PB case: dashed line for isotherm with estimated loading, □ experimental values, ■ average of experimental values. PF case: full line for isotherm with estimated loading, ○ experiments, ● average of experimental values. The dotted lines refers to other water loading values, as reference.

expected, given the 26.5% reduction of sorbent inventory already mentioned in Section 2.

From the observation of the adsorbent particles before and after the experiments, from the shape of the breakthrough profiles, and from the reproducibility of the experiments, it is suggested neither that the different structure of the packing might have caused an additional loss of capacity to adsorb CO_2 for the PF, nor that there might have been some mismatching of the experimental conditions between the two sets of experiments (those performed with PB and those with PF). Therefore, it has been inferred that the loss of capacity is due to a residual amount of water loaded on the sorbent, which could not desorb under the conditions the column had been regenerated at. This is plausible because the zeolite beads used in the PF had been exposed to air for a longer period of time, also due to the different packing procedures; on top of that, the PB only has also been briefly exposed to higher temperatures (up to 200 °C) after being packed in the column, while performing some auxiliary measurements that were necessary for the preparation of the experimental setup.

From the comparison of the adsorbed amounts with the isotherms for CO_2 adsorption over Zeolite 13X pre-loaded with water, computed according to Hefti and Mazzotti [31], the amount of residual water adsorbed is estimated equal to 0.15 and 1.85 mol per kg of adsorbent, for PB and PF respectively, as shown in Fig. 9. The partial pressure of CO_2 shown is the one reached in the column at the end of the breakthrough experiment (after full saturation), where the total pressure of the column was higher than ambient (about 2.3 bar) due to pressure decay downstream of the adsorption bed.

4.2. Regeneration by heating

Fig. 10 shows the temperature and outlet concentration profiles measured during the regeneration. Regeneration has been performed immediately after the breakthrough experiment, in this case heating the column up to 120 °C.

The temperature profiles shown in Fig. 10a confirm the trends observed in the heating experiments with absence of flow, given the small flow rates of released gas recorded at column outlet. The PF configuration allows for significantly faster heating and homogeneous temperature distribution in the radial direction. The desorption wave is more dispersed for the PB, due to the resistance encountered by the heat reaching the center of the bed, as shown by the delay with which the central thermocouple detects a temperature increase. Here heat transfer is so slow that the bed does not reach the thermal steady state by the time the desorption of CO_2 is completed.

In the PF, the heat is quickly transferred to the whole cross section instead. This turns out into a quick release of the adsorbed CO_2, hence the time required for desorption is reduced from 120 min of the PB case to less than 50 min (Fig. 10b).

4.3. Cooling

The last step of the experiment, cooling down to 25 °C, has been performed immediately after regeneration; this is the reason why the temperature in the center of the PB starts from a sensibly lower value compared to that of the PF. Fig. 11 shows the evolution in time recorded by the three thermocouples, while the flow rate at the outlet has not been monitored in this phase, because both column ends have been kept closed.

The dynamics here observed are analogous to those recorded during the heating step.

5. Modeling

To simulate the behavior of the adsorption column with the two different packing configurations, we have resorted to the use of the adsorption process modeling tool developed in house at ETH [34]. The employed dynamic one-dimensional (in the axial coordinate) model has been validated for different sorbents, gas mixtures and process operations on a laboratory scale rig with 2.5 cm diameter columns [29, 34–37].

Due to the sensibly larger diameter of the column used in these study, and the strongly non-uniform temperature distributions observed during the heating experiments, the assumption of negligible radial temperature gradient may be questionable, especially in the PB case.

However, we were interested in testing the capability of the one-dimensional model to reproduce the adsorption breakthrough curves. To partially compensate for the intrinsic inaccuracy of the one-dimensional model, instead of constant heat transfer coefficients we have used coefficient calculated according to literature correlations as function of the bed geometry, the sorbent properties, the fluid dynamics and the thermodynamic properties of the gas mixture. Contextually, two different formulations of the heat transfer coefficients have been used for the PB and PF case, in order to describe the different heat transfer mechanisms involved.

For both packing configurations, a single pseudo-phase accounting for the gas phase, the solid phase and the adsorbed phase is considered, assuming thermal equilibrium among the phases. Therefore a single energy balance for the whole bed can be written, whereas an additional energy balance for the vessel walls is computed, as in Joss et al. [2]. Consistently with the aim of resorting as little as possible to values fitted on the current experiments, the overall heat transfer coefficient bed-to-wall, U_{ov}, has been determined from available validated correlations, as detailed in Sections 5.1 and 5.2. The convective heat transfer coefficient from the external side of the wall to the thermostat fluid has been instead fitted to the profiles of the heating experiments, resulting in a value of 100 $W/m^2/K$.

Regarding the adsorption isotherms for CO_2 and N_2 on Zeolite 13X, the Sips isotherms measured by Hefti et al. [28,31] have been employed in the model, while the heat transfer coefficients for the linear driving force (LDF) kinetic model have been assumed equal to 0.1 and 0.5 s^{-1}, for CO_2 and N_2 respectively, according to the experimental estimates made by Marx et al. [29] on the same sorbent.

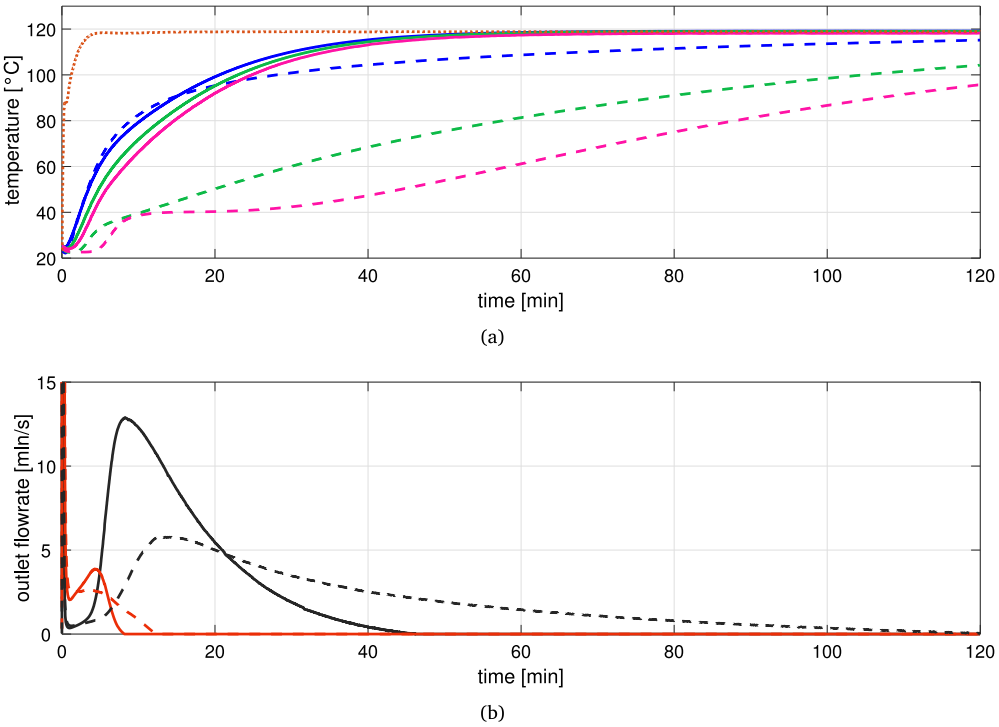

Fig. 10. Regeneration experiment. The bed is heated up to 120 °C while the bottom of the column is left open to allow for gas evacuation. (a) Dynamic evolution of the temperature within the column as measured by the three thermocouples placed at 120 mm from the inlet of the adsorbent bed. The dashed lines indicate the measurements in the packed bed. The full lines indicate the measurements in the packed foam. The colors indicate the position of the thermocouples: central (magenta), half-radius (green) and close to wall (blue). The dotted red line indicates the temperatures of the oil flowing in the jacket. (b) Dynamic evolution of the gas flow rate at outlet, from the combined measurements of the mass flow meter and of the mass spectrometer. The dashed lines indicate the measurement in the packed bed. The full lines indicate the measurement in the packed foam. The colors indicate the two species of the binary mixture, namely CO_2 (black) and N_2 (red).

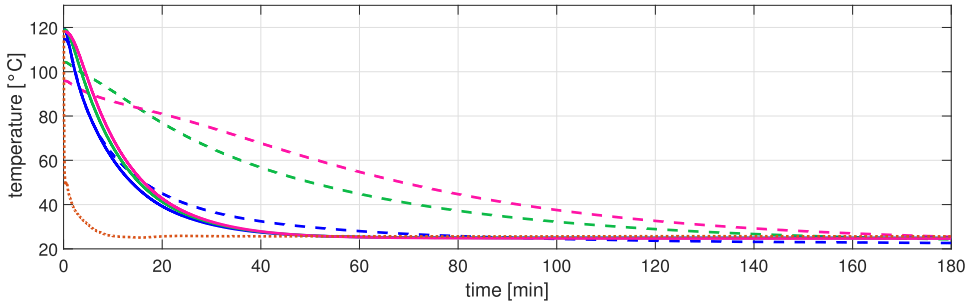

Fig. 11. Dynamic evolution of the temperature within the column as measured by the three thermocouples placed at 120 mm from the inlet of the adsorbent bed. The dashed lines indicate the measurements in the packed bed. The full lines indicate the measurements in the packed foam. The colors indicate the position of the thermocouples: central (magenta), half-radius (green) and close to wall (blue). The dotted red line indicates the temperatures of the oil flowing in the jacket.

5.1. Packed bed

For the PB case, U_{ov} is derived according to Dixon et al. [38] from a series of two thermal resistances, which consider heat transfer at wall and heat transfer through the bed, respectively:

$$\frac{1}{U_{ov,PB}} = \frac{1}{h_{w,PB}} + \frac{D_{in}}{a\, k_{eff,PB}} \tag{2}$$

$$a = 6\,\frac{Bi + 4}{Bi + 3} \tag{3}$$

where the Biot number Bi is calculated as ratio between the heat transfer from the bed to its surroundings and heat transfer within the bed, as follows

$$Bi = \frac{h_{w,PB}\, D_{in}}{2\, k_{eff,PB}} \tag{4}$$

and where $h_{w,PB}$ and $k_{eff,PB}$ are both calculated according to Specchia et al. [39] as sum of a static and a convective term. In particular, considering the interstitial void fraction of the packed bed

$$\varepsilon_{PB} = 1 - \frac{\rho_{PB}}{\rho_p} \tag{5}$$

the two terms are calculated as functions of the velocity of the gas u, of the density ρ_g, of the conductivity k_g, of the viscosity μ_g, and of the heat capacity $c_{p,g}$ of the gas phase, all computed by the model at every time and at every axial position by interpolation from a database on the basis of the gas composition and the gas temperature, according to the following equations:

$$Re = \frac{\rho_g u\, d_p}{\mu_g} \tag{6}$$

$$Pr = \frac{\mu_g c_{p,g}}{k_g} \tag{7}$$

$$Pe = Re\, Pr \tag{8}$$

$$h_{w,PB} = h_{w,PB,static} + h_{w,PB,convective} \tag{9}$$

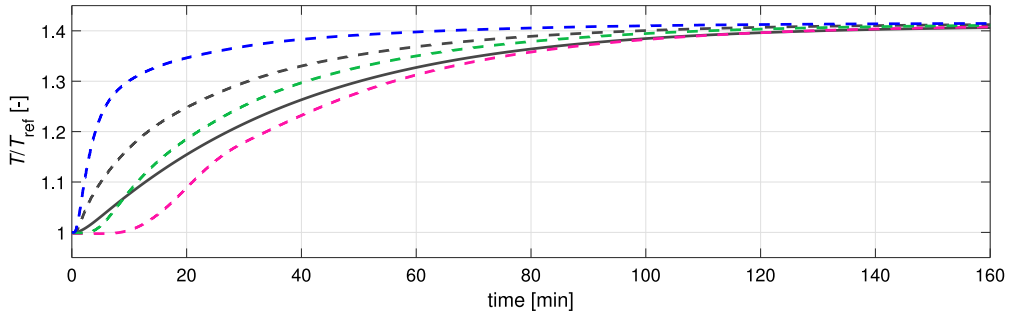

(a) No-flow conditions.

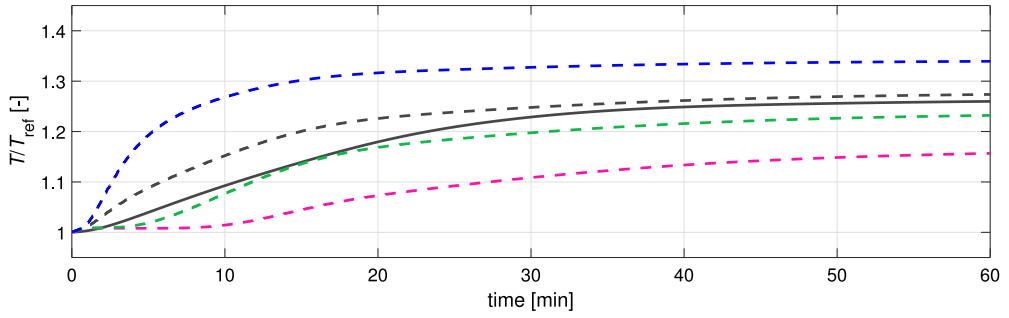

(b) Flow conditions.

Fig. 12. Heating experiment. Comparison of experimental measurements and simulations with the PB configuration. Dynamic evolution of the temperature within the column as measured by the three thermocouples placed at 120 mm from the inlet of the adsorbent bed. The dashed lines indicate the experimental measurements of the thermocouples: central (magenta), half-radius (green) and close to wall (blue). The dashed black line indicates the mixing-cup temperature obtained from the experimental measurements. The full black line indicates the simulation. (a) No-flow conditions: Vacuum. (b) Flow conditions: Ar 25 nL/min.

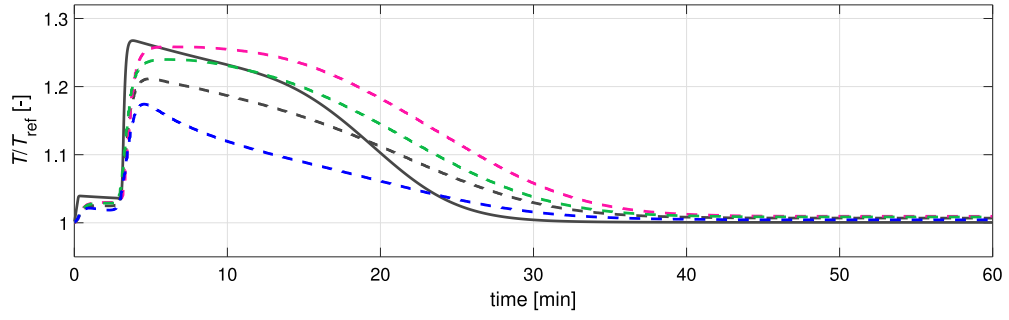

(a)

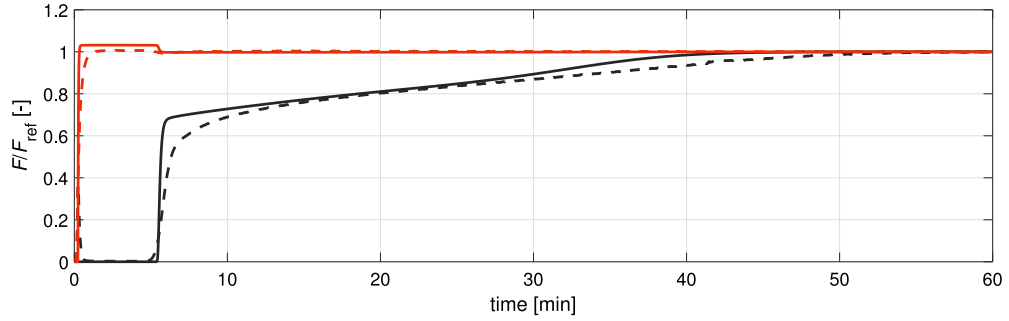

(b)

Fig. 13. Breakthrough experiment. Comparison of experimental measurements and simulations with the PB configuration. (a) Dynamic evolution of the temperature within the column as measured by the three thermocouples placed at 120 mm from the inlet of the adsorbent bed. The dashed lines indicate the experimental measurements of the thermocouples: central (magenta), half-radius (green) and close to wall (blue). The dashed black line indicates the mixing-cup temperature obtained from the experimental measurements. The full black line indicates the simulation. (b) Dynamic evolution of the gas flow rate at outlet. The dashed lines indicate the experimental measurements in the packed bed. The full lines indicate the simulation. The colors indicate the two species of the binary mixture, namely CO_2 (black) and N_2 (red).

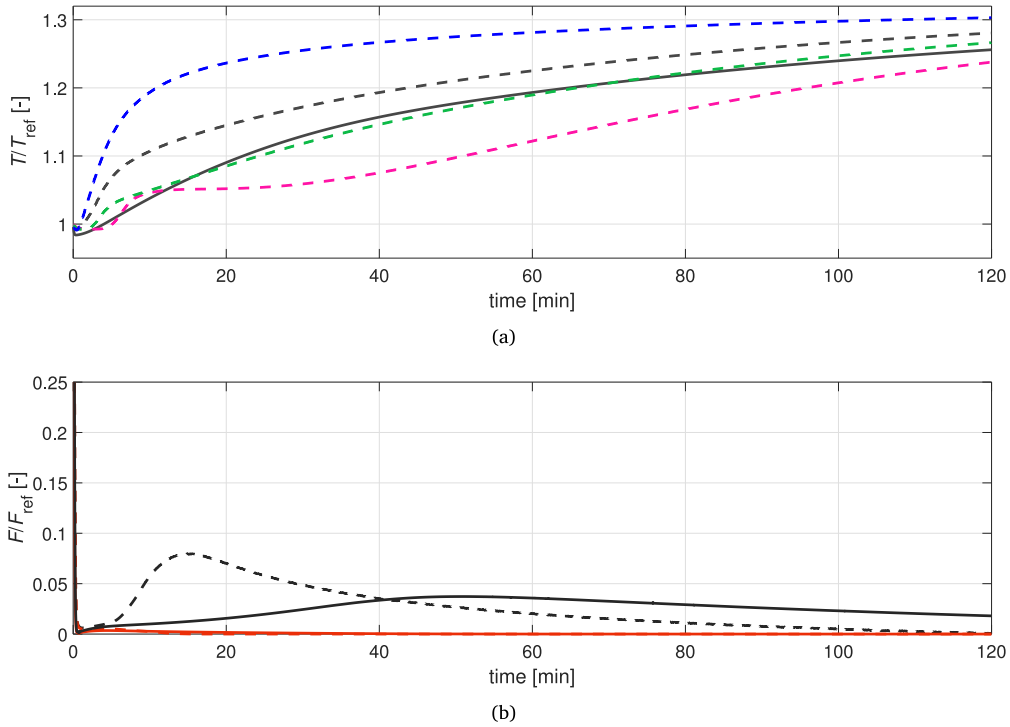

Fig. 14. Regeneration experiment. Comparison of experimental measurements and simulations with the PB configuration. (a) Dynamic evolution of the temperature within the column as measured by the three thermocouples placed at 120 mm from the inlet of the adsorbent bed. The dashed lines indicate the experimental measurements of the thermocouples: central (magenta), half-radius (green) and close to wall (blue). The dotted black line indicates the mixing-cup temperature obtained from the experimental measurements. The full black line indicates the simulation. (b) Dynamic evolution of the gas flow rate at outlet. The dashed lines indicate the experimental measurements in the packed bed. The full lines indicate the simulation. The colors indicate the two species of the binary mixture, namely CO_2 (black) and N_2 (red).

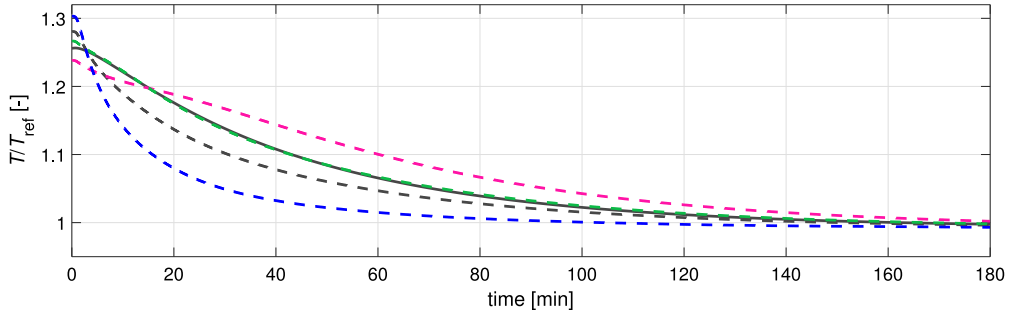

Fig. 15. Comparison of experimental measurements and simulations for a cooling experiment with the PB configuration. Dynamic evolution of the temperature within the column as measured by the three thermocouples placed at 120 mm from the inlet of the adsorbent bed. The dashed lines indicate the experimental measurements of the thermocouples: central (magenta), half-radius (green) and close to wall (blue). The dashed black line indicates the mixing-cup temperature obtained from the experimental measurements. The full black line indicates the simulation.

$$h_{w,PB,static} = \frac{k_g}{d_p}\left(2\varepsilon_{PB} + (1-\varepsilon_{PB})\left(0.0024\left(\frac{D_{in}}{d_p}\right)^{1.58} + \frac{k_g}{3\,k_p}\right)^{-1}\right) \tag{10}$$

$$h_{w,PB,convective} = \frac{k_g}{d_p}\,0.0835\,Re^{0.91}\left(\frac{Pr}{Pr_{ref}}\right)^{\frac{1}{3}} \qquad Re \le 1200 \tag{11}$$

$$h_{w,PB,convective} = \frac{k_g}{d_p}\,1.23\,Re^{0.53}\left(\frac{Pr}{Pr_{ref}}\right)^{\frac{1}{3}} \qquad Re > 1200 \tag{12}$$

where $Pr_{ref} = 0.7018$, and

$$k_{eff,PB} = k_{eff,PB,static} + k_{eff,PB,convective} \tag{13}$$

$$k_{eff,PB,static} = k_g\varepsilon_{PB} + \frac{k_g(1-\varepsilon_{PB})}{0.22\varepsilon_{PB}^2} + \frac{2}{3}\frac{k_g}{k_p} \tag{14}$$

$$k_{eff,PB,convective} = k_g\frac{Pe}{Pe_{ref}} \tag{15}$$

$$Pe_{ref} = 8.65\left(1 + 19.4\left(\frac{d_p}{D_{in}}\right)^2\right) \tag{16}$$

In order to compare the three temperatures measured by thermocouples and the single temperature value calculated by the model, a mixing-cup temperature has been computed from the experimental measurements after fitting the following polynomial expression of the temperature, T, as function of the radial position, r, to the three measured values:

$$T(r) = \alpha + \beta\,r^2 + \gamma\,r^4 \tag{17}$$

where α, β and γ are the three fitting parameters.

Fig. 12 shows the comparison between simulations and measurements for heating only experiments performed in the PB. As foreseen, the prediction capability of the one-dimensional model is limited with this configuration, where the radial effects are pronounced. However,

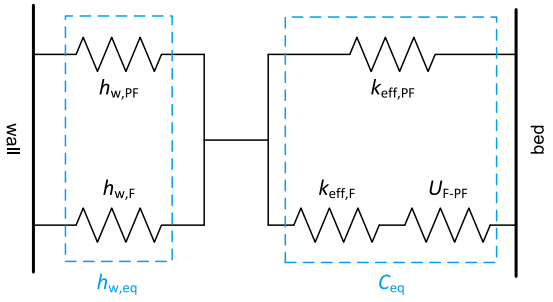

Fig. 16. Graphical representation of the heat transfer mechanism within the packed foam using an equivalent circuit of resistances. Wall and bed are the two poles between which heat is transferred through a series of two thermal resistances, namely $h_{w,eq}$ and C_{eq}, which represent the transfer mechanism at the wall interface and within the bed, respectively. Each resistance consists of two parallel pathways: PF is that of the zeolite beads, F that of the foam.

the model is rather successful in identifying the timing of the temperature transition, as well as the final average temperature reached by the column under flow conditions.

With the above definition of the overall heat transfer coefficient, the one dimensional model has also provided a reasonable prediction of both the temperature and concentration dynamic profiles for the breakthrough experiments, observed differences are compatible with the intrinsic limitation of neglecting any radial gradient. Fig. 13 shows the comparison between the experimental measurements and the simulated profiles for the same breakthrough experiment shown in Fig. 8, with temperature and flow rates expressed in non-dimensional form with reference to the inlet conditions of the gas.

From the comparison it can be seen how the model struggles in predicting the exact shape of the profiles. Also the calculation of the mixing-cup temperature, given its derivation through the fitting of a radial temperature profile, possibly contributes to the misalignment between the temperature profiles due to the strong gradients of the radial profile. Nevertheless, there is an adequate matching in the timing of the temperature and concentration front, as well as in the temperature range observed within the bed. This suggests the one-dimensional model could be use to predict quantitatively the separation performance of the column.

More problematic is instead the simulation of the regeneration step, as shown in Fig. 14, where all properties are again shown in non-dimensional form with reference to the inlet conditions of the adsorption experiment. At the beginning of the regeneration step the two-dimensional effects are pronounced, which translates into particularly large radial temperature gradients. The pattern followed by the heat fluxes, which proceed transversely through the column, causes the more external portion of the bed to release CO_2 earlier, whereas it desorbs later at the core. This is evident from the shape of the temperature fronts in Fig. 14a. As a consequence, a large amount of adsorbate is released before the inner part of the column is actually heated. This effect cannot be represented by the one-dimensional model, where the adsorption dynamics are all dependent on a single averaged temperature. The simulations thus predict a very delayed and excessively distributed desorption front, as shown in Fig. 14b.

As for the cooling step, the matching between model and experiments is somehow satisfying, consistently with the fact that, after regeneration and with both column ends closed, adsorption kinetics are slower and play a minor role in impacting the temperature profiles (Fig. 15).

5.2. Packed foam

For the packed foam instead, the approach suggested by Balzarotti et al. [25] is followed, where an overall heat transfer coefficient, U_{ov} is computed by considering that the metal foam and the adsorbent bed form two separated heat transfer pathways, both at the bed-wall interface and within the bed, as schematically shown in Fig. 16. Inside the bed, the model assumes the presence of a gas/solid resistance between the solid foam and the pellets (represented by U_{F-PF}).

The transfer coefficients $h_{w,PF}$ and $k_{eff,PF}$ are computed analogously to those of the PB case according to Eqs. (9) and (13), while only changing the interstitial void fraction ε consistently with the solid inventory measured for the PF case and taking into account the volume occupied by the metal foam, i.e.

$$\varepsilon_{PF} = 1 - \frac{1}{\varepsilon_F}\frac{\rho_{PF}}{\rho_p} \tag{18}$$

while the terms for the metal foam $h_{w,F}$ and $k_{eff,F}$ are computed as in Aghaei et al. [40] and in Bracconi et al. [26], respectively

$$h_{w,F} = \frac{k_g}{\delta_{gap}} \tag{19}$$

$$\delta_{gap} = 0.00013 + 0.14\, D_{cell} \tag{20}$$

$$k_{eff,F} = \left(\frac{1}{3} + \frac{2}{3}\left(1-\varepsilon_F\right)\right)\left(1-\varepsilon_F\right) k_F \tag{21}$$

where D_{cell} is the average diameter of the foam cells.

As regards the exchange term between metal foam and bed, U_{F-PF}, it is computed by analogy through Eq. (2)

$$\frac{1}{U_{F-PF}} = \frac{1}{h_{w,int}} + \frac{D_{cell}}{a\, k_{eff,int}} \tag{22}$$

where $h_{w,int}$ and $k_{eff,int}$ are calculated as $h_{w,PF}$ and $k_{eff,PF}$, respectively, substituting the column diameter D_{in} with the cell diameter D_{cell}. The Biot number for the calculation of the factor a is also computed accordingly.

The series (h_w and k_{eff}) of parallel (bed and metal foam) heat transfer pathways are then represented by a single overall heat transfer coefficient U_{ov} as

$$\frac{1}{U_{ov,PF}} = \frac{1}{h_{w,eq}} + \frac{1}{C_{eq}} \tag{23}$$

$$h_{w,eq} = h_{w,PF} + h_{w,F} \tag{24}$$

$$C_{eq} = \frac{1}{R_{PF}} + \frac{1}{R_F} \tag{25}$$

$$R_{PF} = \frac{D_{in}}{6.13\, k_{eff,PF}} \tag{26}$$

$$R_F = \frac{D_{in}}{6.13\, k_{eff,F}} + \frac{4}{D_{in}\, S_{V,F}\, U_{F-PF}} \tag{27}$$

where $S_{V,F}$ represents the foam surface per unit volume, computed according to Ambrosetti et al. [41].

As shown by the comparison of simulated and experimental profiles (Fig. 17, the one-dimensional model is very effective in predicting the temperature distribution within the PF, where the radial effects substantially lessen compared to the PB. With the formulation adopted for the heat transfer coefficient within the column, and the estimated value of the wall-to-fluid coefficient for the external side of the wall, the temperature transient is predicted very precisely. This demonstrates that the heat transfer model proposed and validated by Balzarotti et al. [25] on a 30 mm diameter column can be effectively deployed for diameters up to 80 mm.

The one-dimensional model predicts the temperature and concentration profiles with good accuracy, although a minor deviation can be observed from the experimental data in both the height of the temperature front and its spreading. The latter is more pronounced than in the PB case, reasonably due to the combination of an enhanced axial conductivity in the bed and a mild inhomogeneity of the packing density across the cross section, which could not be clearly observed during the packing and unpacking operations though (Fig. 18).

In order to predict the breakthrough time, it is necessary to take into account the residual amount of water loading left on the zeolite

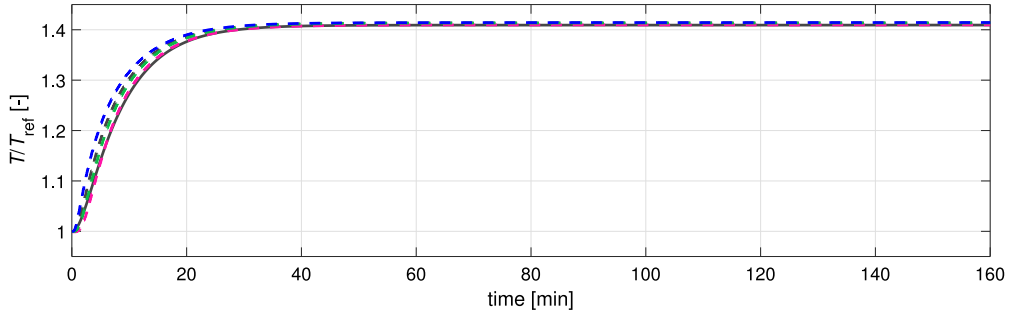

(a) No-flow conditions.

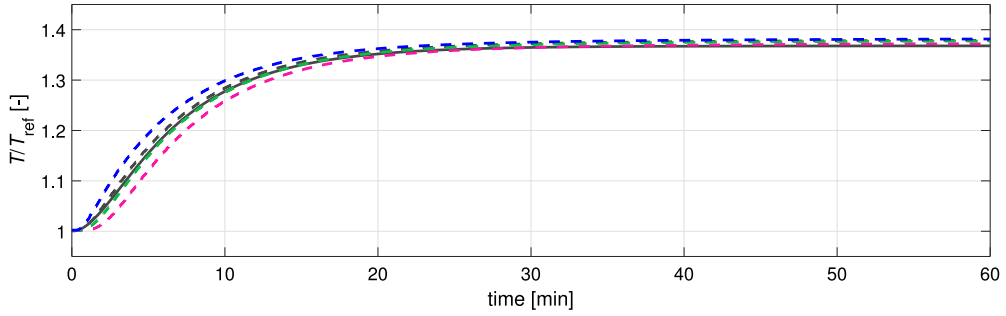

(b) Flow conditions.

Fig. 17. Heating experiment. Comparison of experimental measurements and simulations with the PF configuration. Dynamic evolution of the temperature within the column as measured by the three thermocouples placed at 120 mm from the inlet of the adsorbent bed. The dashed lines indicate the experimental measurements of the thermocouples: central (magenta), half-radius (green) and close to wall (blue). The dashed black line indicates the mixing-cup temperature obtained from the experimental measurements. The full black line indicates the simulation. (a) No-flow conditions: Vacuum. (b) Flow conditions: Ar 25 nL/min.

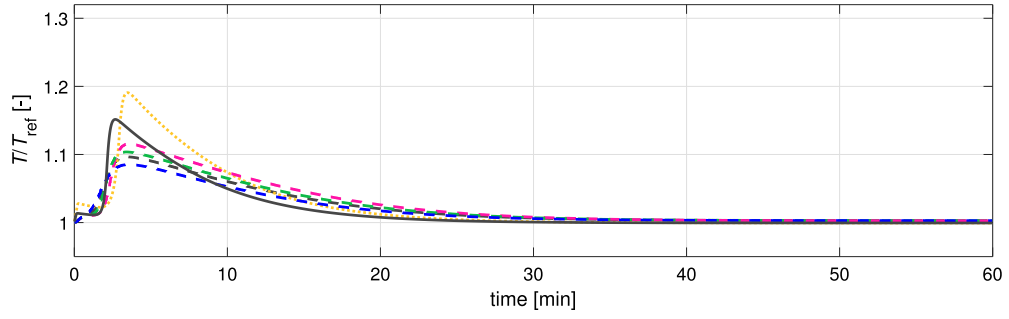

(a)

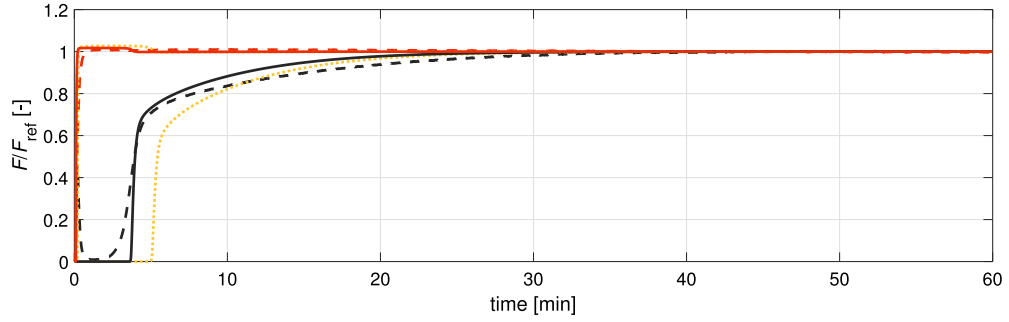

(b)

Fig. 18. Comparison of experimental measurements and simulations for a breakthrough experiment with the PF configuration. (a) Dynamic evolution of the temperature within the column as measured by the three thermocouples placed at 120 mm from the inlet of the adsorbent bed. The dashed lines indicate the experimental measurements of the thermocouples: central (magenta), half-radius (green) and close to wall (blue). The dotted black line indicates the mixing-cup temperature obtained from the experimental measurements. The full black line indicates the simulation, whereas the dotted yellow line indicates the simulation with less residual water loading, as if it were the same of the PB case. (b) Dynamic evolution of the gas flow rate at outlet. The dashed lines indicate the experimental measurements in the packed bed. The full lines indicate the simulation. The colors indicate the two species of the binary mixture, namely CO_2 (black) and N_2 (red). The dotted yellow lines indicate the simulation with less residual water loading.

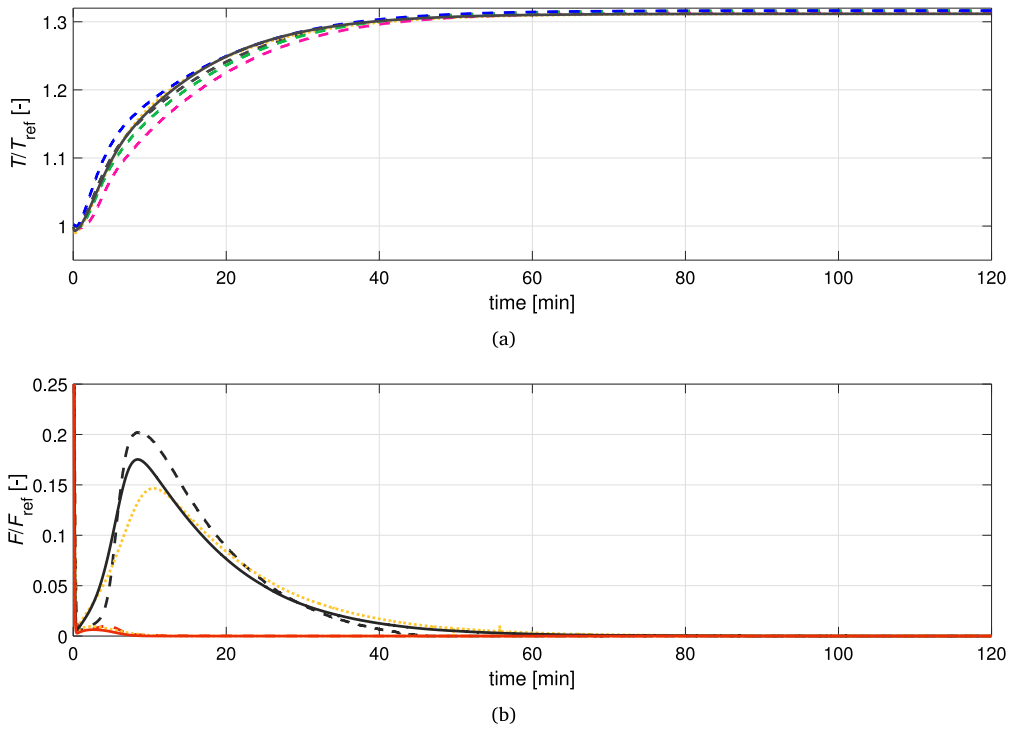

Fig. 19. Comparison of experimental measurements and simulations for a regeneration experiment with the PF configuration. (a) Dynamic evolution of the temperature within the column as measured by the three thermocouples placed at 120 mm from the inlet of the adsorbent bed. The dashed lines indicate the experimental measurements of the thermocouples: central (magenta), half-radius (green) and close to wall (blue). The dashed black line indicates the mixing-cup temperature obtained from the experimental measurements. The full black line indicates the simulation, whereas the dotted yellow line indicates the simulation with less residual water loading, as if it were the same of the PB case. (b) Dynamic evolution of the gas flow rate at outlet. The dashed lines indicate the experimental measurements in the packed bed. The full lines indicate the simulation. The colors indicate the two species of the binary mixture, namely CO_2 (black) and N_2 (red). The dotted yellow lines indicate the simulation with less residual water loading, as if it were the same of the PB case.

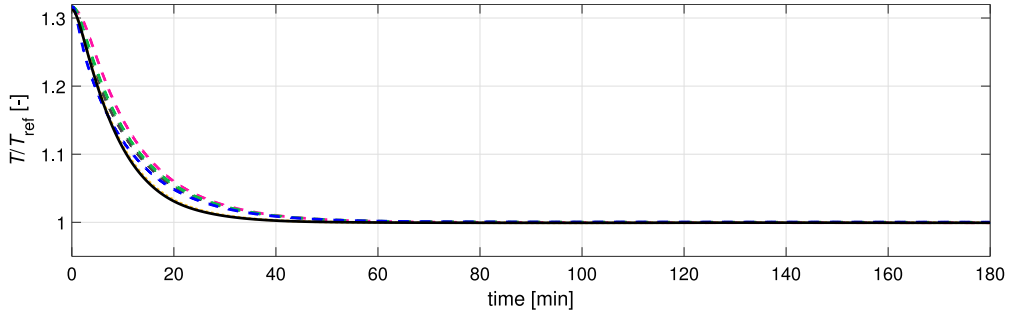

Fig. 20. Comparison of experimental measurements and simulations for a cooling experiment with the PB configuration. Dynamic evolution of the temperature within the column as measured by the three thermocouples placed at 120 mm from the inlet of the adsorbent bed. The dashed lines indicate the experimental measurements of the thermocouples: central (magenta), half-radius (green) and close to wall (blue). The dashed black line indicates the mixing-cup temperature obtained from the experimental measurements. The full black line indicates the simulation, whereas the dotted yellow line indicated the simulation with less residual water loading, as if it were the same of the PB case.

after the regeneration, consistently with the measurement reported in Section 2. The extended Sips isotherms have been adapted according to the adsorption competition between water and the other species. Hence the timing of both temperature and concentration fronts is correctly predicted by the model, as well as the shapes of the concentration shock (adsorption) and wave (desorption), which would diverge more from the experimental ones if a lower residual water loading were considered (Figs. 18b and 19b).

As expected, the flatter radial temperature gradients observed with the PF configuration enable a better prediction of the temperature and concentration profiles during the regeneration steps, than for the PB case.

Good agreement is also found for the cooling step, as shown in Fig. 20. The slight overestimation of the cooling rate by the model is most likely related to the fact that a single wall-to-oil heat transfer coefficient is used for all steps in the model, while heating and cooling are performed in the laboratory rig using two different thermostats that recirculate slightly different oil flow rates.

In order to provide a quantitative reference for the heat transfer enhancement yielded by the PF, the lumped heat transfer coefficients, U_{ov}, for the two configurations are compared in Fig. 21 through the nondimensional Nusselt number, defined as

$$\mathrm{Nu} = \frac{U_{ov}\, D_{in}}{2\, k_g} \tag{28}$$

in analogy with Bastos Rebelo et al. [42], where k_g is the conductivity of the gas phase, in this specific case for pure Argon at 25 °C and 1 atm (1.01325 bar). For the PF configuration, heat transfer is enhanced by a factor 5 under no-flow conditions, and the increase with the Reynolds number of the particle, Re_p, is also steeper than in the PB case.

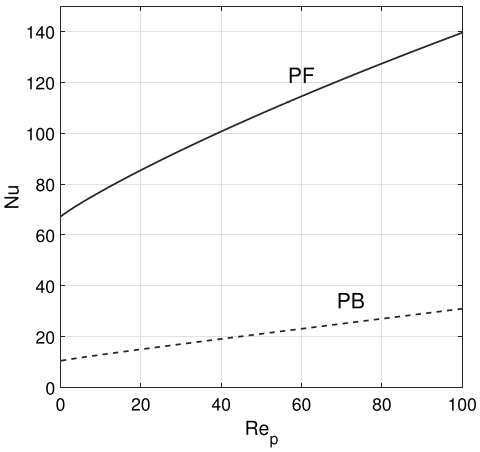

Fig. 21. Comparison of the Nusselt number defined according to Eq. (28) as a function of the Reynolds number of the particle Re_p for the two configurations.

6. Process performance

In order to assess the impact of the introduction of the open-cell foam on the overall process efficiency, PB and PF have been compared in the optimization of a simple 3-step TSA cycle for post-combustion CO_2 capture.

To overcome the issue of the model inaccuracy in predicting the temperature profiles during the heating step with the PB configuration, as discussed in Section 5.1, a column geometry with a diameter of 30 mm is considered, being in line with the column diameters used both for the validations of the adsorption model [29,35,37], and of the model of heat transfer in the foam [25]. Moreover, the lab scale experiments on the 80 mm column have highlighted the development of strong temperature gradients in the case of packed bed, which would lead to a loss of separation performance. Such large cross sections are for this reason commonly avoided in tubular packed beds, although they could be used for PF configurations instead, leading to a likely decrease in the capital cost of the adsorption vessels. For the sake of a fair comparison and a conservative assessment, both configurations are anyway optimized for the same column diameter, namely 30 mm. The heat transfer coefficient for the external side of the column wall has been chosen so as to be representative of an industrial shell-and-tube heat exchanger, in line with other applications of tubular reactors reported in literature [29,43]. The main process parameters used in the optimization are reported in Table 2; the column design and the model parameters do not differ from those used in the simulation of the experiments, unless specified.

The sorbent considered is the same used in the experiments, Zeolite 13X, as well as the composition of the fed CO_2-N_2 mixture, i.e. 12%–88%. The cycle configuration corresponds to the cycle A described by Joss et al. [2], which consists of:

1. an adsorption step at ambient pressure, cooled at 30 °C
2. a regeneration step with the open column bottom, heated at 150 °C
3. a cooling step with closed column, cooled at 30 °C

As reported by Joss et al. this cycle configuration allows reaching neither CO_2 recovery rates much higher than 70%, nor CO_2 purity much higher than 80%. Therefore, the cycle design has been optimized subject to these recovery and purity specifications to minimize the specific process consumption of thermal energy (meant as energy required for heating purposes only, and expressed per unit mass of CO_2 captured) and maximize the process productivity (computed as mass of CO_2 captured per unit mass of adsorbent and per unit cycle time). The two-objective optimization has been performed by means of both a sensitivity analysis and a genetic algorithm optimization, for which MATLAB *gamultiobj* optimizer has been used. Given the trade-off between the two objectives, the optimization has resulted into a set of Pareto-equivalent optima.

Table 2
Parameters used in the multi-objective optimization.

Adsorption column geometry	
Wall thickness	2.5 mm
Inner diameter	30.0 mm
Column length	1500.0 mm
External wall heat transfer coefficient	300 W/m^2/K
Gas feed	
Inlet composition (volumetric)	CO_2/N_2 12.0/88.0%
Inlet temperature	30 °C
Inlet pressure	1.3 bar

Table 3
Optimal cycle configurations.

	PB min. en.	PB max. prod.	PF min. en.	PF max. prod.
Optimal variable values				
t_{ads} [s]	991	489	997	342
t_{reg} [s]	1898	733	1676	417
t_{cool} [s]	1219	380	965	100
$\dot{v}_{feed}$ [m/s]	0.311	0.495	0.241	0.495
Performance				
Recovery [%]	72.8	70.1	70.7	71.7
Purity [%]	87.7	84.7	87.1	82.7
en. cons. [MJ_{th}/kg_{CO2}]	7.07	8.72	8.72	11.5
prod. [$kg_{CO2}/h/t_{ads}$]	63.9	125.1	75.8	226.5

The following design parameters have been considered as optimization variables: (1) the adsorption step duration, t_{ads}; (2) the regeneration step duration, t_{reg}; (3) the cooling step duration, t_{cool}; and (4) the inlet gas volumetric flow rate of a single tube, $\dot{V}_{feed}$, upper-bounded by the limit associated with the minimum fluidization velocity of the adsorbent pellets.

Fig. 22 shows the Pareto fronts obtained from the optimization in the energy-productivity plane.

As expected, the benefit of the PF configuration on the productivity of the process is evident. The maximum productivity achieved with the packed foam is 80% larger than that obtained with the standard fixed bed, which implies that the same flue gas flow rate can be treated with 45% less sorbent. In general, the whole cloud of simulated process designs that meet the separation specifications is shifted toward higher productivity values for the PF case. The reduced duration of the regeneration and cooling steps is the key enabler for this improvement in process performance, as it can be inferred from the value of the optimal cycle design reported in Table 3, corresponding to the two ends of the Pareto front.

However, the increase in process productivity comes at the inevitable cost of a higher energy consumption per unit mass CO_2 captured. This is not surprising, provided that the heat capacity of the two adsorption beds (including the metal foam, where present) per unit mass adsorbent are equal to 920 kJ/kg/K for the PB and 1214 kJ/kg/K for the PF. Provided that the two configurations operate with the same cyclic sorbent capacity for CO_2 and the same inner temperature swing, this would imply that 32% more thermal energy has to be provided to the PF process to capture the same amount of CO_2. The comparison between the two Pareto fronts shows, instead, that the increase in energy consumption for the PF case is of about 23% for the points with the lowest energy consumption. It can be therefore concluded that the improved management of the heat fluxes within the bed also allows for a more efficient consumption of the heat transferred to the sorbent,

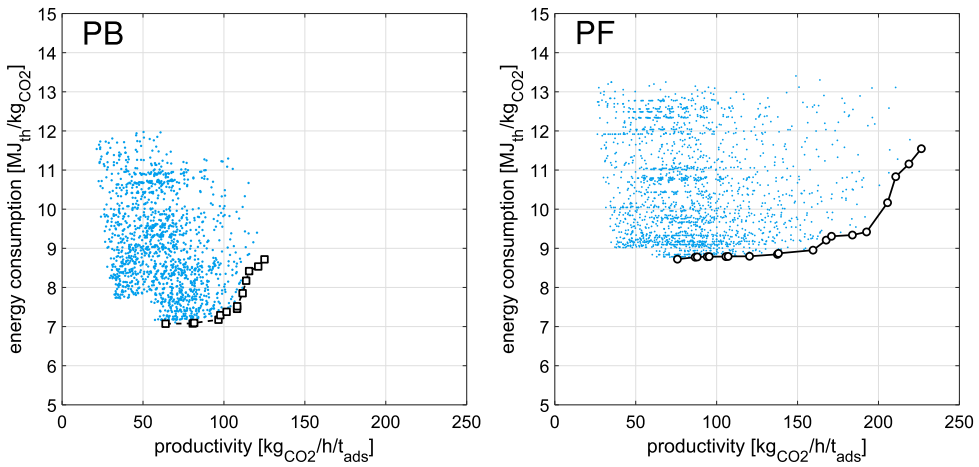

(a) Packed Bed (b) Packed Foam

Fig. 22. Pareto front in the energy-productivity plane for a minimum CO_2 recovery rate of 70% and a minimum captured CO_2 purity of 80%. The blue points represent all the cycle designs, among those simulated, that meet the separation specifications. The black symbols connected by the lines identify the Pareto front.

because the overall energy penalty is lower than the additional thermal requirement associated with the heat capacity of the metal foam. Or, in other words, that with the foam more CO_2 is captured per unit adsorbent mass and unit energy consumed.

In conclusion, determining whether the increase of productivity could be worth the increase in energy consumption may only be possible by means of a detailed cost analysis of the capital and operational expenditure associated with the process, which is beyond the scope of this contribution. However, it can be reasonably guessed that the capital expenditure should cover a large share of the total cost of a TSA, because of the expensive heat exchanging systems integrated in the adsorption columns. Thus, provided that productivity is an effective proxy of the capital cost of a separation unit, the application of packed foam to TSA processes would eventually result into a significant reduction of the total cost. It is also to be considered that an increase of tube diameter, as allowed by the use of the foam, could possibly be conducive to a decrease in equipment costs, thanks to the reduction of the total number of tubes.

7. Conclusions

With the present contribution, the authors have presented experimental and modeling results of the application of conductive open-cell packed foams to temperature swing adsorption processes for CO_2 capture. All results have been assessed in a systematic comparison with the standard bed configuration for TSA separations, i.e. fixed bed of packed pellets.

A first experimental campaign, aimed at measuring heat transfer within the two different bed configurations, has identified a substantial advantage of the packed foam configuration over the standard packed bed in terms of fast heat transfer and homogeneous heat distribution within the column.

A second experimental campaign, dedicated to the reproduction of the main steps of a TSA cycle for CO_2 capture, has highlighted two contrasting features intrinsic to the packed foam configuration: on the one hand, the partial loss of adsorption capacity compared to the packed bed; on the other hand, the reduction of the time required for the regeneration and the cooling of the adsorption bed.

Moreover, a one-dimensional model for the simulation of adsorption processes, properly modified to account for the different heat transfer regime observed in the packed foam, has been tested against the experimental measurements to assess its prediction accuracy. It has been concluded that the accuracy of the model is good, both qualitatively and quantitatively, for all those cases where limited radial temperature gradients are developed in the adsorption vessel.

Finally, the model has been applied to a two-objective optimization of the process design of a simple TSA process for CO_2 capture, aimed at minimum energy consumption and maximum process productivity. The results obtained from the optimization demonstrate that the TSA process with the packed foam achieves significantly larger (+80%) process productivity, at the expenses of a mildly higher energy consumption (+23%).

Declaration of competing interest

The authors declare that they have no known competing financial interests or personal relationships that could have appeared to influence the work reported in this paper.

Acknowledgment

The authors from Politecnico di Milano acknowledge the European Research Council for Grant Agreement 694910/INTENT: “Structured Reactors with Intensified Energy Transfer for Breakthrough Catalytic Technologies”.

References

[1] J. Mérel, M. Clausse, F. Meunier, Carbon dioxide capture by indirect thermal swing adsorption using 13X zeolite, Environ. Prog. 25 (4) (2006) 327–333, URL https://doi.org/10.1002/ep.10166.

[2] L. Joss, M. Gazzani, M. Mazzotti, Rational design of temperature swing adsorption cycles for post-combustion CO_2 capture, Chem. Eng. Sci. 158 (September 2016) (2017) 381–394, URL https://doi.org/10.1016/j.ces.2016.10.013.

[3] R.P. Lively, R.R. Chance, B.T. Kelley, H.W. Deckman, J.H. Drese, C.W. Jones, W.J. Koros, Hollow fiber adsorbents for CO_2 removal from flue gas, Ind. Eng. Chem. Res. 48 (15) (2009) 7314–7324, URL https://doi.org/10.1021/ie9005244.

[4] T. Gupta, R. Ghosh, Rotating bed adsorber system for carbon dioxide capture from flue gas, Int. J. Greenh. Gas Control 32 (2015) 172–188, URL https://doi.org/10.1016/j.ijggc.2014.10.020.

[5] R. Veneman, Z. Li, J. Hogendoorn, S. Kersten, D. Brilman, Continuous CO_2 capture in a circulating fluidized bed using supported amine sorbents, Chem. Eng. J. 207–208 (2012) 18–26, URL https://doi.org/10.1016/j.cej.2012.06.100.

[6] T. Pröll, G. Schöny, G. Sprachmann, H. Hofbauer, Introduction and evaluation of a double loop staged fluidized bed system for post-combustion CO_2 capture using solid sorbents in a continuous temperature swing adsorption process, Chem. Eng. Sci. 141 (2016) 166–174, URL https://doi.org/10.1016/j.ces.2015.11.005.

[7] R.P. Ribeiro, C.A. Grande, A.E. Rodrigues, Electric swing adsorption for gas separation and purification: A review, Sep. Sci. Technol. 49 (13) (2014) 1985–2002, URL https://doi.org/10.1080/01496395.2014.915854.

[8] A. Ntiamoah, J. Ling, P. Xiao, P.A. Webley, Y. Zhai, CO_2 capture by temperature swing adsorption: Use of hot CO_2-rich gas for regeneration, Ind. Eng. Chem. Res. (2015) URL https://doi.org/10.1021/acs.iecr.5b01384.

[9] E. Meloni, M. Martino, P. Pullumbi, F. Brandani, V. Palma, Intensification of TSA processes using a microwave-assisted regeneration step, Chem. Eng. Process. - Process Intensif. 160 (2021) 108291, URL https://doi.org/10.1016/j.cep.2020.108291.

[10] A. Kodama, T. Kuma, M. Goto, T. Tsutomu, H. Hirose, Experimental study of optimal operation for a honeycomb adsorber operated with thermal swing, J. Chem. Eng. Japan 26 (5) (1993) 530–535, URL https://doi.org/10.1252/jcej.26.530.

[11] F.D. Yu, L.A. Luo, G. Grévillot, Electrothermal desorption using joule effect on an activated carbon monolith, J. Environ. Eng. 130 (3) (2004) 242–248, URL https://doi.org/10.1061/(asce)0733-9372(2004)130:3(242).

[12] D. Menard, X. Py, N. Mazet, Activated carbon monolith of high thermal conductivity for adsorption processes improvement: Part A: Adsorption step, Chem. Eng. Process. - Process Intensif. 44 (9) (2005) 1029–1038, URL https://doi.org/10.1016/j.cep.2005.02.002.

[13] F. Rezaei, P. Webley, Structured adsorbents in gas separation processes, Sep. Purif. Technol. 70 (3) (2010) 243–256, URL https://doi.org/10.1016/j.seppur.2009.10.004.

[14] N. Hedin, L. Andersson, L. Bergström, J. Yan, Adsorbents for the post-combustion capture of CO_2 using rapid temperature swing or vacuum swing adsorption, Appl. Energy 104 (2013) 418–433, URL https://doi.org/10.1016/j.apenergy.2012.11.034.

[15] B. Verougstraete, A. Martín-Calvo, S. Van der Perre, G. Baron, V. Finsy, J.F. Denayer, A new honeycomb carbon monolith for CO_2 capture by rapid temperature swing adsorption using steam regeneration, Chem. Eng. J. 383 (2020) 123075, URL https://doi.org/10.1016/j.cej.2019.123075.

[16] J. Chen, P. Bollini, V. Balakotaiah, Oxidative dehydrogenation of ethane over mixed metal oxide catalysts: Autothermal or cooled tubular reactor design? AIChE J. (November 2020) (2021) 1–13, URL https://doi.org/10.1002/aic.17168.

[17] E. Tronconi, G. Groppi, C.G. Visconti, Structured catalysts for non-adiabatic applications, Curr. Opin. Chem. Eng. 5 (2014) 55–67, URL https://doi.org/10.1016/j.coche.2014.04.003.

[18] F. Kapteijn, J.A. Moulijn, Structured catalysts and reactors – Perspectives for demanding applications, Catal. Today (October) (2020) URL https://doi.org/10.1016/j.cattod.2020.09.026.

[19] T. Boger, M. Menegola, Monolithic catalysts with high thermal conductivity for improved operation and economics in the production of phthalic anhydride, Ind. Eng. Chem. Res. 44 (1) (2005) 30–40, URL https://doi.org/10.1021/ie040088f.

[20] M. Iwaniszyn, K. Sindera, A. Gancarczyk, M. Korpyś, R.J. Jędrzejczyk, A. Kołodziej, P.J. Jodłowski, Experimental and CFD investigation of heat transfer and flow resistance in woven wire gauzes, Chem. Eng. Process. - Process Intensif. (ISSN: 02552701) 163 (September 2020) (2021) URL https://doi.org/10.1016/j.cep.2021.108364.

[21] R. Balzarotti, A. Beretta, G. Groppi, E. Tronconi, A comparison between washcoated and packed copper foams for the intensification of methane steam reforming, React. Chem. Eng. 4 (8) (2019) 1387–1392, URL https://doi.org/10.1039/c9re00125e.

[22] A. Egana, O. Sanz, D. Merino, X. Moriones, M. Montes, Fischer-Tropsch synthesis intensification in foam structures, Ind. Eng. Chem. Res. 57 (31) (2018) 10187–10197, URL https://doi.org/10.1021/acs.iecr.8b01492.

[23] M. Iovane, R. Zennaro, P. Forzatti, G. Groppi, L. Lietti, E. Tronconi, C.G. Visconti, S. Rossini, E. Mignone, inventors. ENI S.p.A., Rome, Italy, assignee, Reactor for exothermic or endothermic catalytic reactions, 2016, US patent 9, 387, 456 B2.

[24] L. Fratalocchi, C.G. Visconti, G. Groppi, L. Lietti, E. Tronconi, Intensifying heat transfer in Fischer-Tropsch tubular reactors through the adoption of conductive packed foams, Chem. Eng. J. 349 (2018) 829–837, URL https://doi.org/10.1016/j.cej.2018.05.108.

[25] R. Balzarotti, M. Ambrosetti, A. Beretta, G. Groppi, E. Tronconi, Investigation of packed conductive foams as a novel reactor configuration for methane steam reforming, Chem. Eng. J. 391 (2020) URL https://doi.org/10.1016/j.cej.2019.123494.

[26] M. Bracconi, M. Ambrosetti, M. Maestri, G. Groppi, E. Tronconi, A fundamental analysis of the influence of the geometrical properties on the effective thermal conductivity of open-cell foams, Chem. Eng. Process. - Process Intensif. 129 (2018) 181–189, URL https://doi.org/10.1016/j.cep.2018.04.018.

[27] R. Ostuni, A. Guarino, S. Ravasio, U. Rossi, G. Groppi, E. Tronconi, M. Ambrosetti, inventors. Casale SA, Lugano, Switzerland, assignee, Adsorber suitable for temperature swing adsorption, 2019, Patent WO/2019/025407.

[28] M. Hefti, D. Marx, L. Joss, M. Mazzotti, Adsorption equilibrium of binary mixtures of carbon dioxide and nitrogen on zeolites ZSM-5 and 13X, Microporous Mesoporous Mater. 215 (2015) 215–226, URL https://doi.org/10.1016/j.micromeso.2015.05.044.

[29] D. Marx, L. Joss, M. Hefti, M. Mazzotti, Temperature swing adsorption for post-combustion CO_2 capture: Single- and multicolumn experiments and simulations, Ind. Eng. Chem. Res. 55 (5) (2016) 1401–1412, URL https://doi.org/10.1021/acs.iecr.5b03727.

[30] M. Ambrosetti, M. Bracconi, M. Maestri, G. Groppi, E. Tronconi, Packed foams for the intensification of catalytic processes: assessment of packing efficiency and pressure drop using a combined experimental and numerical approach, Chem. Eng. J. 382 (2020) 1–6, URL https://doi.org/10.1016/j.cej.2019.122801.

[31] M. Hefti, M. Mazzotti, Postcombustion CO_2 capture from wet flue gas by temperature swing adsorption, Ind. Eng. Chem. Res. 57 (45) (2018) 15542–15555, URL https://doi.org/10.1021/acs.iecr.8b03580.

[32] C.G. Visconti, G. Groppi, E. Tronconi, Highly conductive "packed foams": A new concept for the intensification of strongly endo- and exo-thermic catalytic processes in compact tubular reactors, Catal. Today 273 (2016) 178–186, URL https://doi.org/10.1016/j.cattod.2016.02.060.

[33] M. Ambrosetti, G. Groppi, W. Schwieger, E. Tronconi, H. Freund, Packed periodic open cellular structures – an option for the intensification of non-adiabatic catalytic processes, Chem. Eng. Process. - Process Intensif. 155 (6) (2020) 108057, URL https://doi.org/10.1016/j.cep.2020.108057.

[34] N. Casas, J. Schell, R. Pini, M. Mazzotti, Fixed bed adsorption of CO_2/H2 mixtures on activated carbon: experiments and modeling, Adsorption 18 (2012) 143–161.

[35] J. Schell, N. Casas, D. Marx, M. Mazzotti, Precombustion CO 2 capture by pressure swing adsorption (PSA): Comparison of laboratory PSA experiments and simulations, Ind. Eng. Chem. Res. 52 (24) (2013) 8311–8322, URL https://doi.org/10.1021/ie3026532.

[36] N. Casas, J. Schell, R. Blom, M. Mazzotti, MOF and UiO-67/MCM-41 adsorbents for pre-combustion CO_2 capture by PSA: Breakthrough experiments and process design, Sep. Purif. Technol. 112 (2013) 34–48, URL https://doi.org/10.1016/j.seppur.2013.03.042.

[37] A. Streb, M. Mazzotti, Adsorption for efficient low carbon hydrogen production: part 2—Cyclic experiments and model predictions, Adsorption (2021) URL https://doi.org/10.1007/s10450-021-00308-w.

[38] A.G. Dixon, An improved equation for the overall heat transfer coefficient in packed beds, Chem. Eng. Process. - Process Intensif. 35 (5) (1996) 323–331, URL https://doi.org/10.1016/0255-2701(96)80012-2.

[39] V. Specchia, G. Baldi, S. Sicardi, Heat transfer in packed bed reactors with one phase flow, Chem. Eng. Commun. 4 (1980) 361–380, URL https://doi.org/10.1080/00986448008935916.

[40] P. Aghaei, C.G. Visconti, G. Groppi, E. Tronconi, Development of a heat transport model for open-cell metal foams with high cell densities, Chem. Eng. J. 321 (2017) 432–446, URL https://doi.org/10.1016/j.cej.2017.03.112.

[41] M. Ambrosetti, M. Bracconi, G. Groppi, E. Tronconi, Analytical geometrical model of open cell foams with detailed description of strut-node intersection, Chem.-Ing.-Tech. 89 (7) (2017) 915–925, URL https://doi.org/10.1002/cite.201600173.

[42] N.F. Bastos Rebelo, K.A. Andreassen, L.I. Suarez Ríos, J.C. Piquero Camblor, H.J. Zander, C.A. Grande, Pressure drop and heat transfer properties of cubic iso-reticular foams, Chem. Eng. Process. - Process Intensif. 127 (2018) 36–42, URL https://doi.org/10.1016/j.cep.2018.03.008.

[43] J. Bremer, K. Sundmacher, Operation range extension via hot-spot control for catalytic CO_2 methanation reactors, React. Chem. Eng. 4 (6) (2019) 1019–1037, URL https://doi.org/10.1039/c9re00147f.